© 2017. Published by The Company of Biologists Ltd | Development (2017) 144, 1425-1440 doi:10.1242/dev.143362

STEM CELLS AND REGENERATION

RESEARCH ARTICLE

Notch signalling restricts inflammation and *serpine1* expression in the dynamic endocardium of the regenerating zebrafish heart

Juliane Münch[1,2], Dimitrios Grivas[1,3], Álvaro González-Rajal[1,4], Rebeca Torregrosa-Carrión[1,3] and José Luis de la Pompa[1,3,*]

ABSTRACT

The zebrafish heart regenerates after ventricular damage through a process involving inflammation, fibrotic tissue deposition/removal and myocardial regeneration. Using 3D whole-mount imaging, we reveal a highly dynamic endocardium during cardiac regeneration, including changes in cell morphology, behaviour and gene expression. These events lay the foundation for an initial expansion of the endocardium that matures to form a coherent endocardial structure within the injury site. We studied two important endocardial molecules, Serpine1 and Notch, which are implicated in different aspects of endocardial regeneration. Notch signalling regulates developmental gene expression and features of endocardial maturation. Also, Notch manipulation interferes with attenuation of the inflammatory response and cardiomyocyte proliferation and dedifferentiation. *serpine1* is strongly expressed very early in the wound endocardium, with decreasing expression at later time points. *serpine1* expression persists in Notch-abrogated hearts, via what appears to be a conserved mechanism. Functional inhibition studies show that Serpine1 controls endocardial maturation and proliferation and cardiomyocyte proliferation. Thus, we describe a highly dynamic endocardium in the regenerating zebrafish heart, with two key endocardial players, Serpine1 and Notch signalling, regulating crucial regenerative processes.

KEY WORDS: Heart regeneration, Endocardium, Myocardium, Signalling, Serpine1, Notch

INTRODUCTION

The adult mammalian heart fails to regenerate after cardiac injury owing to a permanent deposition of massive fibrotic tissue, together with the inability to replenish lost cardiac muscle (Conrad et al., 1995). The zebrafish exhibits a remarkable capacity for organ regeneration (Gemberling et al., 2013). Localised damage to the zebrafish heart using the cryoinjury model induces processes similar to those in the infarcted mammalian heart: cell death, inflammatory cell infiltration and scar deposition. In fish, this scar is dissolved and the injured tissue is replaced by new cardiomyocytes (González-Rosa et al., 2011; Schnabel et al., 2011; Chablais and Jazwinska, 2012b). Most studies have focused on how cardiomyocyte dedifferentiation and proliferation are achieved to regenerate cardiac muscle (Kikuchi et al., 2010; Fang et al., 2013; Aguirre et al., 2014; Kikuchi, 2015), but how different cardiac tissues interact to orchestrate heart regeneration is poorly understood. Ventricular resection rapidly activates the epicardium and endocardium, and endocardial retinoic acid is required for cardiomyocyte proliferation (Kikuchi et al., 2011). However, the behaviour and function of the endocardium after cryoinjury have not been investigated.

Endocardial Notch signalling regulates cardiomyocyte proliferation, differentiation and patterning in a non-cell-autonomous manner during mouse cardiac chamber development (Grego-Bessa et al., 2007; Luxán et al., 2013; D'Amato et al., 2016). Notch function in the damaged adult mouse heart is unclear; it has been suggested to control fibrotic and regenerative repair in a pressure-overload model (Nemir et al., 2014), but is unable to promote cardiomyocyte proliferation after myocardial infarction (Felician et al., 2014).

Here, we study the behaviour and morphology of the endocardium after cryoinjury, using three-dimensional (3D) confocal imaging to visualise the complete injured region. Our results revealed activated, proliferating and migrating endocardial cells at 3 days post cryoinjury (dpci), in contrast to the more mature, less proliferative, coherent endocardial structure in the injury site at 7 dpci. Furthermore, we describe the consequences of Notch manipulation on endocardial morphology, attenuation of the inflammatory response and cardiomyocyte proliferation. We also establish Serpine1 as an early endocardial injury-response factor, with regulatory roles in cellular maturation and proliferation. Our findings highlight the significance of endocardial signals regulating different processes during heart regeneration.

RESULTS

Endocardial cells reside and expand within the injured tissue after cryoinjury

To study the endocardium during heart regeneration we used the endocardial enhancer trap line *ET33-mi60a*, in which GFP is inserted close to the promoter of the Notch signalling modulator *lunatic fringe* (*lfng*) (Poon et al., 2010). We used the cryoinjury model of heart regeneration that faithfully recapitulates mammalian ischemic injury (Chablais et al., 2011; González-Rosa et al., 2011; Schnabel et al., 2011). We detected GFP expression throughout the ventricle but also within the cryoinjury site of *ET33-mi60a* hearts (Fig. 1A,B; sample sizes for all figures are provided in Tables S1, S2). GFP^+ cells (*GFP* mRNA, Fig. 1C) expressed the endothelial erythroblast transformation-specific transcription factor Erg (Fig. 1D, Fig. S1A) and the endocardial development gene *nfatc1a* (Fig. 1E, Fig. S1B) (Larson et al., 2004; Wong et al., 2012). This suggests that GFP^+ cells in the wound endocardium

[1]Intercellular Signalling in Cardiovascular Development and Disease Laboratory, Centro Nacional de Investigaciones Cardiovasculares Carlos III (CNIC), Melchor Fernández Almagro 3, Madrid E-28029, Spain. [2]Institute of Biochemistry and Biology, Potsdam University, Karl-Liebknecht-Straße 24-25, Potsdam D-14476, Germany. [3]CIBER CV, 28029 Madrid, Spain. [4]Cancer Division, Garvan Institute of Medical Research, The Kinghorn Cancer Centre, 370 Victoria Street, Darlinghurst NSW 2010, Australia.

*Author for correspondence (jlpompa@cnic.es)

J.L.d., 0000-0001-6761-7265

Received 12 August 2016; Accepted 20 February 2017

Development (2017) 144, 1425-1440 doi:10.1242/dev.143362

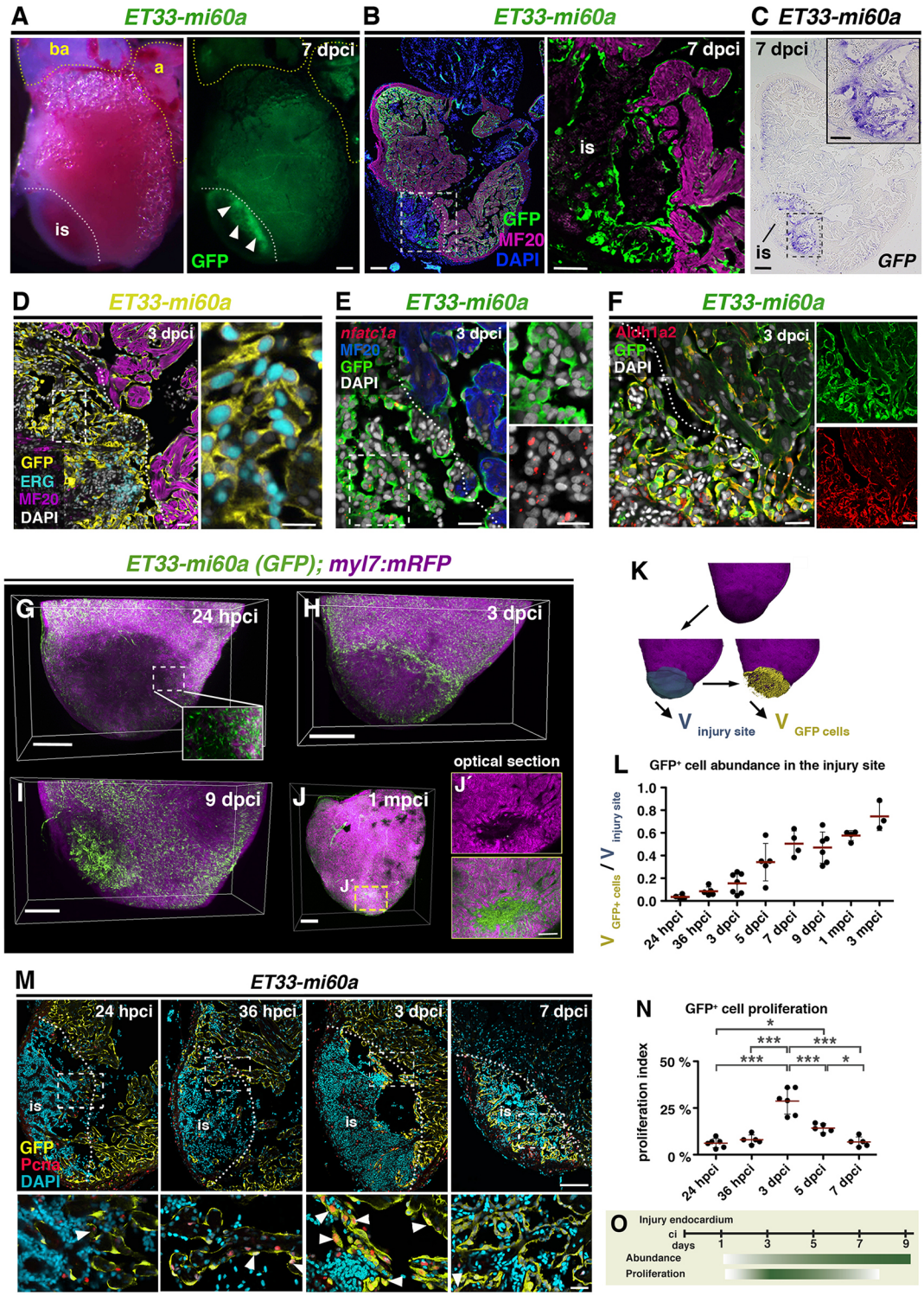

Fig. 1. The endocardium expands at the injury site. (A) *ET33-mi60a* transgenic zebrafish heart, whole-mount views. Strong GFP expression is apparent in the cryoinjured region of the ventricle (arrowheads). (B) *ET33-mi60a* heart section. Immunohistochemistry (IHC) shows GFP$^+$ endocardial cells in a myosin heavy chain (MF20)$^-$ area. (C) *ET33-mi60a* heart consecutive section to Fig. 1B showing *GFP* ISH. (D-F) IHC, or IHC combined with FISH. GFP$^+$ cells express Erg (D), *nfatc1a* (E) and Aldh1a2 (F). (B-F) Boxed areas are magnified on the right. (G-I) Volume rendering of *ET33-mi60a;myl7:mRFP* injured ventricles. Endocardium, green; myocardium, magenta. (J,J′) Volume rendering (J) and amplified optical section from the centre (J′) of an injured ventricle. (K) Imaris-based volume quantification. The volume of the mRFP$^-$ region was determined (blue, $V_{injury\ site}$) and used as a mask to label GFP$^+$ cells in this region (yellow) and determine their volume ($V_{GFP\ cells}$). (L) Scatter plot showing the relative volume occupied by GFP$^+$ cells in the injury site. Mean (red line)±s.d.; one-way ANOVA and Newman-Keuls test (see Table S3). (M) IHC showing Pcna$^+$ GFP$^+$ endocardial nuclei (arrowheads). Boxed areas magnified beneath. (N) Scatter plot showing percentage of Pcna$^+$ cells among GFP$^+$ cells within and adjacent (50 µm) to the injury site. Mean±s.d.; one-way ANOVA and Newman-Keuls test, **P*<0.05, ****P*<0.005 (see Table S4). (O) Schematic illustrating that endocardium proliferation precedes endocardial expansion at the injury site. is, injury site; a, atrium; ba, bulbus arterious. Dotted lines demarcate injured tissue. Scale bars: 200 µm in A-C,G-J; 20 µm in D-F; 100 µm in M; 50 µm in magnified views in B,C; 20 µm in magnified views in D,E,M; 100 µm in J.

Development (2017) 144, 1425-1440 doi:10.1242/dev.143362

region retain their endocardial/endothelial features after injury and are activated. These GFP$^+$ wound endocardial cells expressed Aldh1a2 protein (Fig. 1F), consistent with previous results (Kikuchi et al., 2011). Likewise, the endocardial reporter *Tg(fli1a:GFP)* (Lawson and Weinstein, 2002) presented GFP$^+$ cells in the injury site (Fig. S1C).

We studied wound endocardium dynamics by high-resolution 3D confocal imaging. Optical clearing of *ET33-mi60a;myl7:mRFP* hearts by CUBIC (clear, unobstructed brain imaging cocktails and computational analysis; reagent 1; Susaki et al., 2014) allowed detection of endogenous fluorescence signals: GFP in the endocardium and membrane-bound RFP in cardiomyocytes (Rohr et al., 2008). At 24 hours post cryoinjury (hpci), strongly reduced mRFP fluorescence at the injury site relative to uninjured tissue indicated the absence of myocardial cells (Fig. 1G, Movie 1). Despite the overall reduced GFP fluorescence, we detected spared GFP$^+$ cells within the injury site (Fig. 1G, Movie 1). To estimate the abundance of endocardial cells with respect to the injury site extension, we used Imaris software to 3D reconstruct confocal images and quantify the volume of the injury site, identified by the absence of mRFP$^+$ cardiomyocytes (Fig. 1K; see Materials and Methods). We also quantified the volume of the injury site occupied by GFP$^+$ cells (Fig. 1K). The relationship between these two values provided an estimate of the relative volume occupied by GFP$^+$ endocardial cells over the course of regeneration (Fig. 1K,L). GFP$^+$ cells in an uninjured region, surrounding cardiomyocytes, occupied a volume of 46.1±2% (Fig. S1D). At 24 hpci, GFP$^+$ cells were rare at the injury site, occupying 3.5±2.1% of the injured volume (Fig. 1G,L, Fig. S1D, Movie 1). By 36 hpci, the GFP$^+$ volume increased slightly but significantly (8.5±3.8%; Fig. 1L, Fig. S1E, Movie 2). At 3 dpci, most hearts exhibited a higher occupation by GFP$^+$ cells (15.5±8.9%; Fig. 1H,L, Movie 3). The proportion of the injured volume occupied by GFP$^+$ cells progressively increased until 7 dpci (Fig. 1L, Fig. S1E, Movies 4, 5) and was stable at 9 dpci (47.1±13.7%; Fig. 1I,L, Movie 6). The relative volume occupied by GFP$^+$ cells continued to increase up to 3 months post cryoinjury (mpci), albeit more gradually (57.6±4.4% at 1 mpci and 74.6±12.6% at 3 mpci; Fig. 1J,L, Fig. S1E, Movies 7, 8). This might be due to the decrease in the total size of the injury site over this period of time (Fig. S1F), when cardiomyocytes had already begun to replace lost cardiac muscle (Fig. 1J, 1 mpci; Fig. S1E, 3 mpci), consistent with published data (Chablais et al., 2011; Itou et al., 2012). Analysis of optical sections in 1 mpci hearts revealed that regions still lacking cardiomyocytes were filled with endocardial cells (Fig. 1J). Moreover, endocardial volume at 1 mpci and 3 mpci is beyond the value of an uninjured region of the heart (Fig. 1L, Fig. S1C), indicating that endocardial density is augmented at the injury site.

We next examined endocardial cell proliferation in *ET33-mi60a* hearts. GFP$^+$ endocardial cells stained for proliferating cell nuclear antigen (Pcna) were very rare in uninjured hearts (Fig. S1G; 0.45±0.15 cells/heart section). At 24 and 36 hpci, several GFP$^+$ endocardial cells at the injury site were Pcna$^+$ (Fig. 1M,N). At 3 dpci, we observed a massive proliferative response of GFP$^+$ cells adjacent to (Fig. 1M, N) and throughout (Fig. S1H) the injury site. Endocardial proliferation decreased at 5 dpci (Fig. 1N, Fig. S1I) and was almost abolished at 7 dpci (Fig. 1M,N). This shows that the highest proliferation coincides with the initiation of endocardial expansion and suggests that endocardial cell proliferation at 3 and 5 dpci contributes to the endocardial expansion from 3 to 7 dpci (Fig. 1O). The observation that maximal endocardial proliferation (3 dpci) occurs before the peak of myocardial proliferation (7 dpci) (Kikuchi et al., 2010; Sallin et al., 2014; Bednarek et al., 2015), and the presence of the endocardium at the injury site throughout regeneration (Kikuchi et al., 2010; Sallin et al., 2014; Bednarek et al., 2015), suggest that endocardial regeneration precedes myocardial regeneration.

Wound endocardium is highly dynamic during regeneration

We next analysed endocardial morphology at different time points after cryoinjury and conducted 3D imaging analysis at high magnification. In the undamaged region of the heart, a coherent network of endocardial cells with elongated morphology surrounded clusters of cardiomyocytes (Fig. 2A). Injury site endocardial cells at 24 hpci were similarly elongated (Fig. 2A). By contrast, we observed a dense and disorganised endocardial mesh at the injury site at 3 dpci (Fig. 2A). Endocardial cells appeared rounded, in clusters and displayed numerous filopodia-like protrusions (Fig. 2A, arrowheads). These co-stained with phalloidin (Fig. 2B, Fig. S2A), indicating an actin-rich cytoskeleton, one characteristic of filopodia (Mallavarapu and Mitchison, 1999; Mattila and Lappalainen, 2008). The high density of GFP$^+$ cells was maintained at 9 dpci; however, cells seemed more orderly aligned than at 3 dpci, forming a coherent sheet (Fig. 2A). Moreover, filopodia-like protrusions were less abundant at 9 dpci than at 3 dpci (Fig. 2C,D).

We next examined expression of the endothelial cell-cell adhesion protein Cadherin 5 (Cdh5), which is involved in endocardial junction integrity (Mitchell et al., 2010). *In situ* hybridisation (ISH) showed strong *cdh5* expression at the injury site, which was weaker throughout the ventricle and in the uninjured heart (Fig. S2B,C). We conducted fluorescent ISH (FISH) on *ET33-mi60a* heart sections and compared levels of *cdh5* mRNA fluorescence of remote and wound endocardium (Fig. 2E,F). Relative *cdh5* expression at the injury site increased up to 1.156 (±0.089) at 3 dpci (Fig. 2G), and even more at 7 dpci (1.820±0.142), indicating that injury endocardium maturation coincides with increasing levels of *cdh5* expression (Fig. 2G). Also, more mature injury endocardium at 7 dpci was strongly associated with collagen fibres at 7 dpci, but not at 3 dpci (Fig. S2D,E).

The presence of filopodia-like protrusions, a characteristic of migrating cells (Ridley, 2011), together with the observed endocardial expansion suggested endocardial cellular migration within the injury site. To test this, we cultured cryoinjured hearts and performed live imaging of the regenerating endocardium in *ET33-mi60a* transgenic fish at ∼2-3 dpci. We observed that endocardial cells changed their location and that individual cells migrated short distances within the injury site (Fig. 2H,I, Movies 9, 10). We also detected endocardial cells sending out filopodia (Fig. 2I, Movie 10).

Overall, we show by morphological, gene expression and live imaging analyses a dynamic post-injury endocardium (Fig. 2J), and distinguish an early activated, proliferative endocardium (3 dpci) from a more mature, organised, less-proliferative endocardial structure (7-9 dpci).

Notch pathway elements are expressed in the endocardium and are implicated in endocardial maturation and heart regeneration

Next, we examined the involvement of Notch, a crucial endocardial cell signalling pathway during development and regeneration (Raya et al., 2003; Zhang et al., 2013; Luxán et al., 2016), in the cryoinjured heart. The ligand Delta-like 4 (Dll4) is expressed in GFP$^+$ wound endocardial cells in *ET33-mi60a* and *Tg(fli1a:GFP)* hearts (Fig. 3A, Fig. S3A,E). *notch1b* expression was initially low

Development (2017) 144, 1425-1440 doi:10.1242/dev.143362

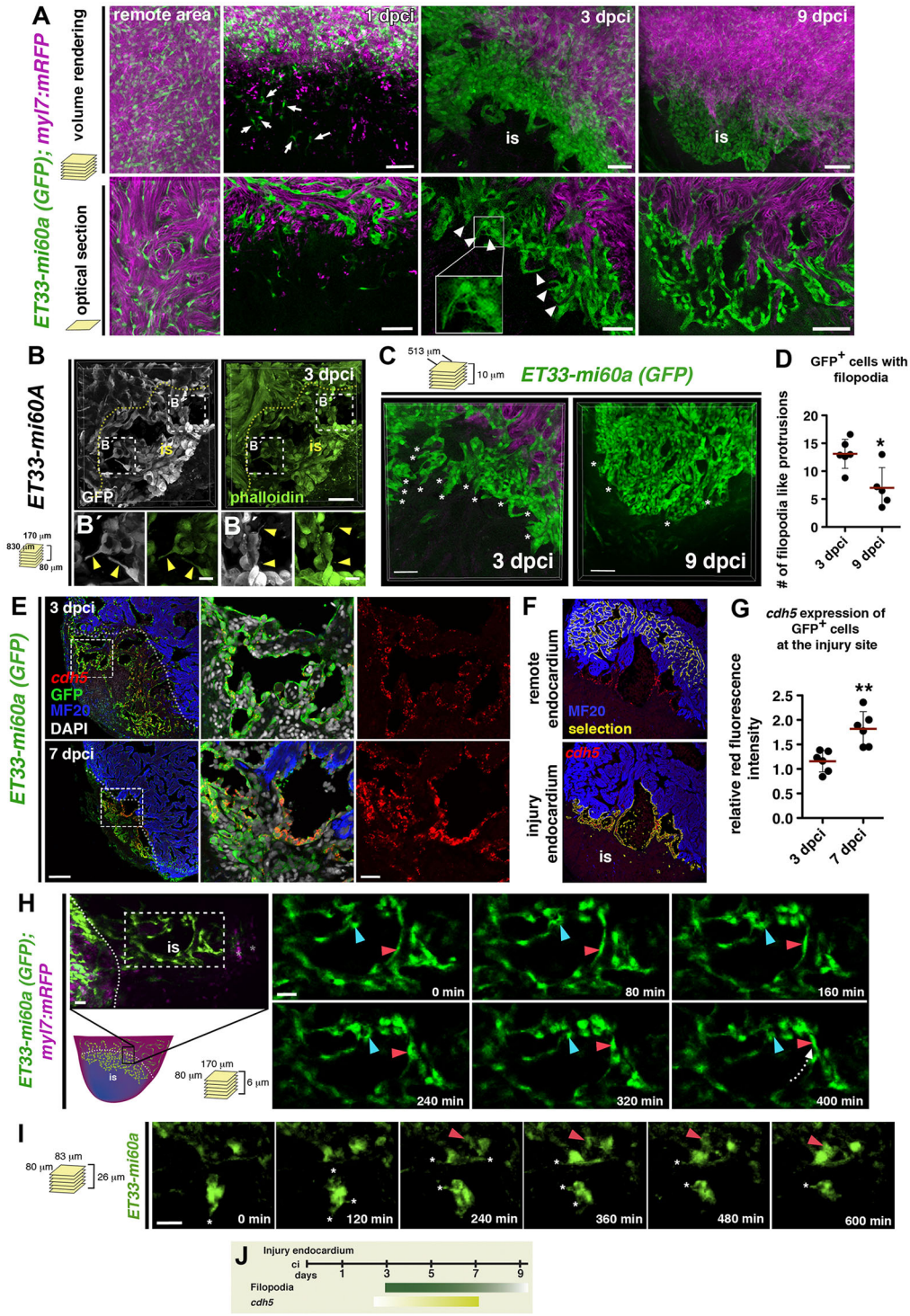

Fig. 2. Characteristics of injury endocardium at different stages of regeneration. (A) Volume rendering and corresponding optical sections of part of the remote and injured region from *ET33-mi60a;myl7:mRFP* hearts. Remote region contains elongated and coherent GFP$^+$ cells. At 1 dpci individual GFP$^+$ cells are seen at the injury site (is) (arrows). At 3 dpci, dense, clustered endocardial cells with filopodia-like protrusions (arrowheads) are observed. At 9 dpci the endocardial cells are more organised, aligned and mostly lack filopodia-like protrusions. (B-B″) Vibratome section of *ET33-mi60a* heart stained for GFP and with phalloidin (for F-actin). Filopodia-like protrusions of wound endocardial cells show phalloidin staining (arrowheads). (C) Volume rendering of part of the injured region from *ET33-mi60a;myl7:mRFP* hearts. (D) Quantification of filopodia-like protrusions from comparable 3D images. Mean±s.d.; *t*-test, **P*<0.05. (E) FISH combined with IF showing high *cdh5* expression (red) in GFP$^+$ wound endocardium. Boxed areas magnified on the right. (F,G) *cdh5* (red) fluorescence intensity measurements with ImageJ software: GFP$^+$ endocardium was selected (F, yellow) in the remote or wound region. Scatter plot (G) showing relative red fluorescence intensity comparing values of both regions. Mean±s.d.; *t*-test, ***P*<0.01. (H,I) Confocal still pictures from time-lapse movies (Movies 9, 10) of wound endocardial cells in cultured *ET33-mi60a;myl7:mRFP* hearts. The box in the schematic indicates the imaging region. Endocardial cells move (H,I, red arrowheads) and change their position (H, blue arrowhead). Dotted arrow (H) indicates the direction of cell migration. Endocardial cells present dynamic filopodia-like protrusions (I, asterisks). (J) Schematic showing wound endocardium characteristics. Filopodia-like protrusions are more abundant at early (3 dpci) than at later (9 dpci) phases. *cdh5* expression increases when regeneration proceeds. Scale bars: 50 µm in A-C; 100 µm in E; 20 µm H,I; 10 µm in magnified views of B.

Development (2017) 144, 1425-1440 doi:10.1242/dev.143362

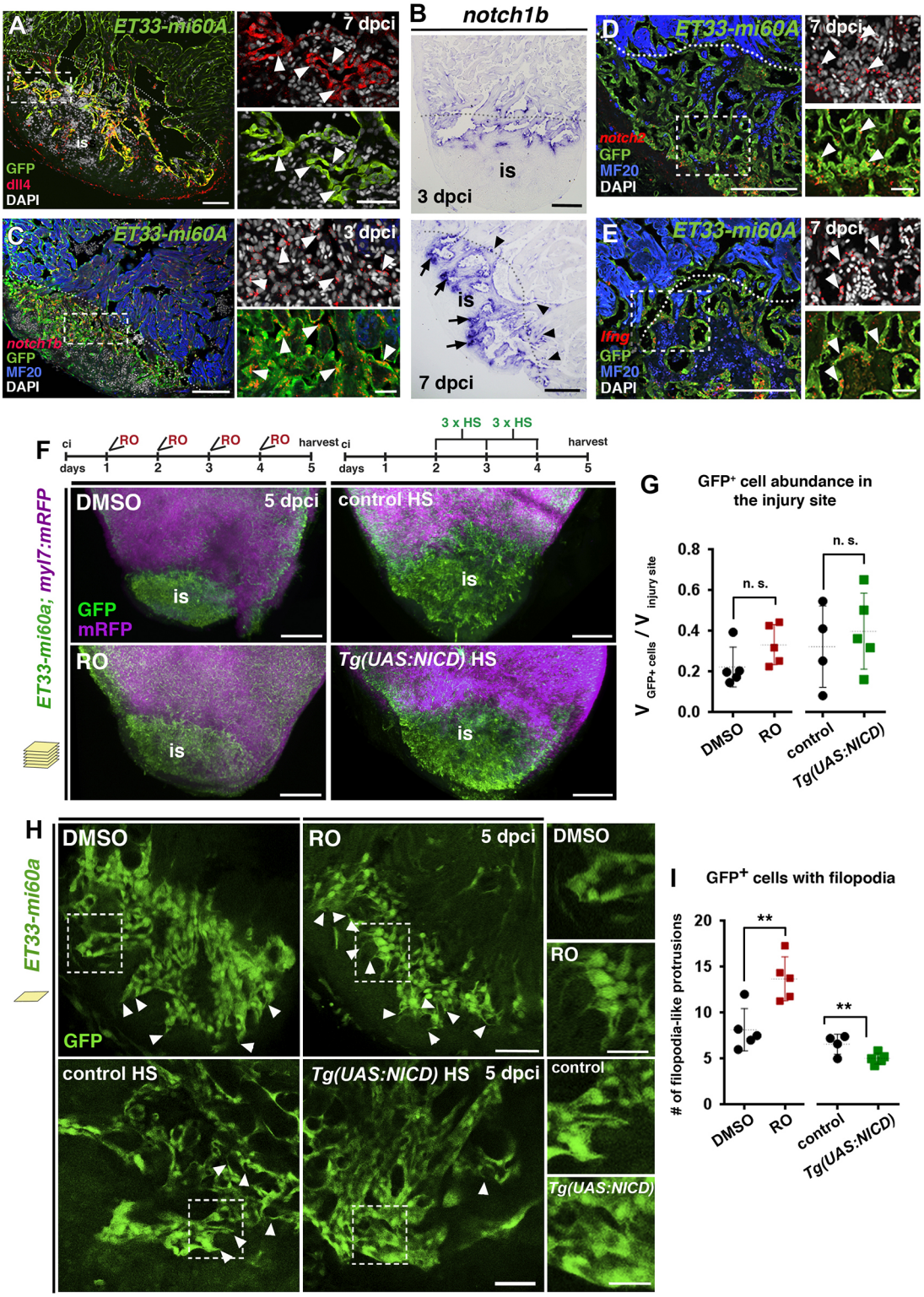

Fig. 3. Notch signalling elements are expressed in the endocardium and Notch signalling modulation affects injury endocardium maturation. (A) IHC showing Dll4 expression by GFP$^+$ wound endocardial cells (arrowheads). (B) ISH showing *notch1b* expression in endocardial cells at the injury site (arrows) and lining injury-adjacent cardiomyocytes (arrowheads). (C-E) FISH for *notch1b* (C), *notch2* (D) or *Ifng* (E) combined with IHC showing transcripts in GFP$^+$ wound endocardial cells (arrowheads). (F) Volume rendering of injured *ET33-mi60a;myl7:mRFP* ventricles after DMSO or RO treatment and of heat shocked (HS) *Tg(UAS:NICD);ET33-mi60a;myl7:mRFP* and control hearts. Treatment regimens are indicated at the top. (G) Scatter plot presenting relative wound GFP$^+$ cell volume. Mean (dotted line)±s.d.; *t*-test. (H) Injury site optical sections showing the disorganisation and clustered appearance of endocardial cells and more filopodia-like protrusions (arrowheads) after RO treatment, and fewer filopodia-like protrusions after heat shock in *Tg(UAS:NICD);ET33-mi60a;myl7:mRFP* hearts. (I) Scatter plot showing the number of filopodia-like protrusions. For representative images used for quantification see Fig. S6A. Mean±s.d.; *t*-test $^{**}P<0.05$. Dotted lines (A,C,D,E) delineate the injury site (is). Boxed areas are magnified on the right. Scale bars: 100 µm in A-E; 200 µm in F; 50 µm in H; 20 µm in magnified views in A,C,D,E; 25 µm in magnified views in H.

Development (2017) 144, 1425-1440 doi:10.1242/dev.143362

(36 hpci, Fig. S3B), but strong *notch1b*, *notch2*, *notch3* and *lfng* transcription was evident in endocardial cells lining injury-adjacent cardiomyocytes and within the injury site at 3 and 7 dpci (Fig. 3B, Fig. S3C,D). FISH combined with immunofluorescence (IF) confirmed *notch1b*, *notch2* and *lfng* expression by GFP^+ wound endocardial cells in *ET33-mi60a* (Fig. 3C-E) and *Tg(fli1a:GFP)* (Fig. S3F) transgenic fish.

To study the requirement of Notch for cryoinjured heart regeneration, we used the γ-secretase inhibitor RO492909 (RO), which effectively reduces Notch activity in the zebrafish embryo and adult fin (Munch et al., 2013), and in the retina (Conner et al., 2014). In the injured heart, RO treatment diminished Notch target gene transcription (Fig. S4A) and impaired heart regeneration, as indicated by the increased amount of fibrotic tissue at 30 dpci (Fig. S4B,C), similar to observations made in the ventricular resection model (Zhao et al., 2014).

We examined the impact of increased Notch activity on regeneration using the inducible model *Tg(hsp70l:Gal4);Tg(UAS:myc-notch1a-intra)* [abbreviated to *Tg(UAS:NICD)*]. Heat shocks induced the expression of the Notch intracellular domain (NICD) (Scheer et al., 2001) and increased Notch target gene transcription in *Tg(UAS:NICD)* injured hearts (Fig. S4D). Differences in regeneration between control and *Tg(UAS:NICD)* hearts were not evident until 33 dpci (Fig. S4E,F), presumably owing to heat shock-induced slowing of regeneration (Gemberling et al., 2013). At 90 dpci, *Tg(UAS:NICD)* hearts retained more fibrotic tissue than control fish (Fig. S4G,H), suggesting that long-term Notch overactivation impairs heart regeneration.

Next, we examined the requirement of Notch for wound endocardial cell expansion and maturation. In line with published results (Zhao et al., 2014), manipulation of Notch signalling did not interfere with endocardial activation (Kikuchi et al., 2011), as shown by unchanged expression of *aldh1a2* (Fig. S5A,B), and did not alter endocardial cell proliferation at 3 dpci (Fig. S5C-E). In *ET33-mi60a* transgenic fish, GFP expression was unaffected by RO treatment or Notch pathway overactivation (Fig. S5G), allowing us to use this line for the following studies.

Notch signalling inhibition for 4 dpci did not significantly alter GFP^+ wound endocardium expansion, which was similar in *Tg(UAS:NICD);ET33-mi60a* and control hearts (Fig. 3F,G). Analysis of endocardial cell morphology in RO-treated hearts at 5 dpci revealed clustered endocardial cells at the injury site (Fig. 3H), similar to our observations at 3 dpci (Fig. 2A). DMSO-treated hearts, however, exhibited a more orderly aligned injury endocardium (Fig. 3H), indicating that endocardial maturation had occurred in control but not in RO-treated hearts. Quantification of filopodia-like protrusions as one characteristic of the early immature wound endocardium (Fig. 2C,D) revealed a higher abundance in RO-treated hearts (Fig. 3H,I, Fig. S6A). Moreover, overactivation of the Notch pathway in *Tg(UAS:NICD);ET33-mi60a* hearts resulted in a reduced number of filopodia-like protrusions (Fig. 3H,I, Fig. S6A), suggesting a role for Notch in endocardial maturation. Additionally, *cdh5* transcript levels, analysed as before (Fig. 2F), did not significantly differ after Notch signalling manipulation (Fig. S6B-E). Thus, these results indicate that a precise level of Notch activation is crucial for heart regeneration after cryoinjury and that Notch is involved in regulating endocardial maturation.

Decreased Notch signalling affects endothelial, cardiovascular and wound healing processes

To study the molecular changes resulting from Notch abrogation in the cryoinjured heart, we extracted RNA from the injured region of the ventricle after RO or DMSO treatment at 3 dpci (Fig. 4A). RNA-seq analysis identified 347 differentially expressed genes, 196 of which were upregulated and 151 downregulated (Fig. 4B, Table S6). Ingenuity-based gene ontology (GO) classification revealed that Notch signalling inhibition affected genes involved in various endothelial cell processes (Fig. 4C), suggesting a function for Notch in endocardial cells, since they are specialised endothelial cells and both cell types share structural and functional genes (Harris and Black, 2010). Furthermore, genes required in the cardiovascular system and for wound healing were dysregulated (Fig. 4C). GO assignments of differentially expressed genes to categories related to endothelial cells, the cardiovascular system and wound healing are indicated in Fig. S7A.

Notch inhibition dysregulated genes involved in the regulation of angiogenesis (*vegfc*, *id1*, *efnb2a*, *egr1*), endothelial integrity [*cldn5b*, *heg* (*heg1*)] and endothelial cell differentiation (*klf2a*, *klf2b*, *aqp1a.1*) (Fig. 4D). A subset of these (*efnb2a*, *heg*, *klf2a*, *egr1*, *id1*) are also endocardial genes (Mably et al., 2003; Grego-Bessa et al., 2007; Vermot et al., 2009; Zhao et al., 2011) and were expressed at the inner border of the injured heart (*egr1*, *id1*; Fig. S7B, C). Confirming the Notch signalling attenuation (Fig. S4A), RNA-seq detected the downregulation of *efnb2a* and *bmp10*, two Notch-dependent genes involved in chamber development (Grego-Bessa et al., 2007) (Fig. 4D). Three additional endocardial genes, *heg*, *klf2a* and *klf2b*, were upregulated upon Notch inhibition (Fig. 4D). *heg* regulates endothelial/endocardial integrity (Kleaveland et al., 2009) and growth of the zebrafish myocardium (Mably et al., 2003). *klf2* gene endothelial expression is induced by shear forces and is related to a stretched, less migratory, differentiated endothelial phenotype (Dekker et al., 2002, 2006). *klf2a* and *heg* transcripts were present in a subset of GFP^+ wound endocardial cells and also in the remote region (Fig. 4E,F), the latter being consistent with previous reports after ventricular resection (Kikuchi et al., 2011).

qPCR analysis confirmed that Notch inhibition increased *heg*, *klf2a* and *klf2b* expression (Fig. 4G) and that Notch overactivation attenuated *heg* expression (Fig. S7D). Moreover, *heg* and *klf2a* expression, which is normally restricted to non-chamber endocardium during cardiac development (DMSO, Fig. 4H) (Mably et al., 2003; Vermot et al., 2009), was expanded to the ventricular endocardium after Notch inhibition (RO, Fig. 4H), suggesting that Notch regulates these genes similarly during development and regeneration.

Notch signalling inhibition alters the expression of inflammatory genes and leads to increased inflammatory cell abundance

RNA-seq analysis revealed the involvement of Notch in cardiovascular and wound healing processes, which led us to study both more in detail. The expression of extracellular matrix (ECM)-degrading proteases [*ctsba*, *ctssb.1* (*ctss2.1*), *mmp9*] and hyaluronidase 2 (*hyal2*), which degrades hyaluronan (Chowdhury et al., 2013), was increased in Notch-diminished hearts (Fig. 5A). Notch inhibition (Fig. 5B) also led to increased expression of inflammatory markers and regulators (*ptgs2b*, *pde7a*, *sgpl1*) (Smith et al., 2003; Ogryzko et al., 2014) and the pro-inflammatory endothelial genes *arg2* (Ryoo et al., 2008) and *tnfrsf9a* (CD137) (Olofsson et al., 2008; Teijeira et al., 2012) (Fig. 5B). This upregulation of inflammatory factors is consistent with the augmented protease gene expression because protease-induced low molecular weight ECM molecule fragments trigger pro-inflammatory signals and leukocyte recruitment (Frangogiannis, 2008; Dobaczewski et al., 2010).

Development (2017) 144, 1425-1440 doi:10.1242/dev.143362

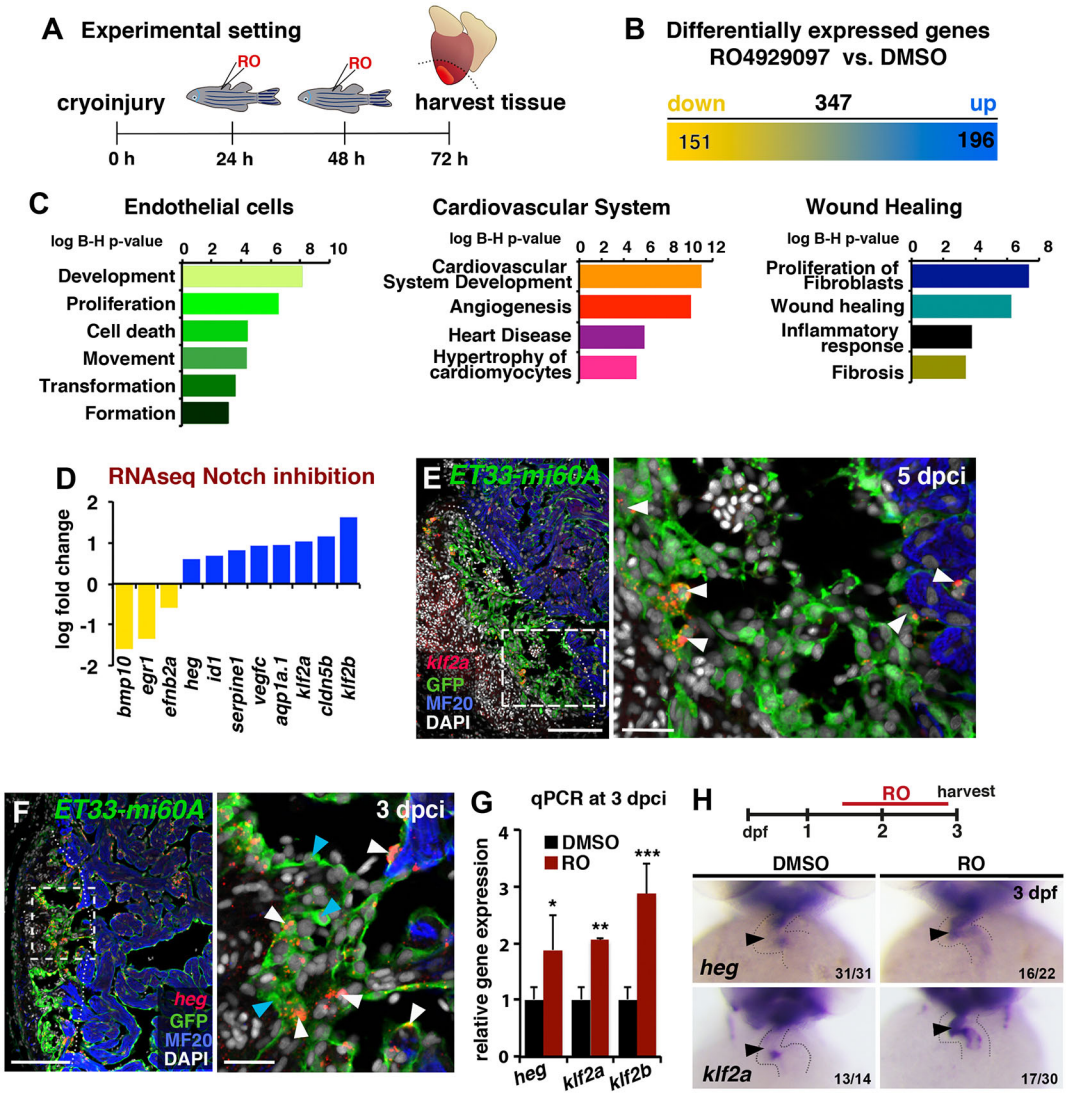

Fig. 4. Notch inhibition affects developmental and injury-related endocardial/endothelial genes. (A) RO injection and RNA extraction procedure from the ventricular apex (below the dotted line). (B) RNA-seq detected 347 genes differentially expressed in injured hearts after RO treatment (fold change >0.5, P<0.05). (C) Ingenuity-based RNA-seq data analysis. The charts represent selected Ingenuity categories affected. (D) RNA-seq revealed differential cardiac expression of endothelial genes at 3 dpci in RO- or DMSO-treated fish. Yellow, downregulated; blue, upregulated. (E,F) FISH against *klf2a* (E) or *heg* (F) combined with IHC. Mosaic expression of both genes was observed in wound and wound-adjacent GFP$^+$ endocardial cells (arrowheads). Boxed areas are magnified on the right. (G) qPCR analysis of *heg*, *klf2a* and *klf2b* expression in injured hearts. Mean±s.d.; *t*-test, *P<0.05, **P<0.01, **P<0.005. (H) ISH in embryos at 3 days post fertilisation (dpf). RO treatment (regime indicated at top) expanded ventricular expression of *heg* and *klf2a* (arrowhead). Dotted lines delineate injury site. The number of embryos displaying the illustrated phenotype among the total number examined is indicated. Scale bars: 100 µm in E,F; 20 µm in magnified views in E,F.

In zebrafish, injured cardiac tissue is infiltrated by immune cells (Schnabel et al., 2011; Wang et al., 2011; Han et al., 2014) but little is known about the timely regulation of inflammatory signals in the cryoinjured heart. qPCR analysis revealed that inflammatory and ECM degradation genes were strongly upregulated at 36 hpci, with levels declining thereafter to reach near-baseline levels at 7 dpci (Fig. 5C,D). ISH revealed *ctssb.1*, *mmp9* and *tnfrsf9a* transcription at the inner injury border after cryoinjury (Fig. S8A,B). We detected inflammatory cells, indicated by *l-plastin* (*lcp1*) or *mpeg1* expression (Herbomel et al., 1999; Ellett et al., 2011), mainly in the injury site and most of these macrophages were in close proximity to GFP$^+$ endocardial cells in *ET33-mi60a* fish (Fig. 5E,F, Fig. S8C). We hypothesize that the early activated wound endocardium may be involved in the regulation of inflammatory cell recruitment, and investigated the function of Notch in this process.

High inflammatory gene expression (Fig. 5C,D) temporally coincided with the high number of *l-plastin*-expressing leukocytes at the inner injury border (Fig. S8D) and low Notch expression at 36 hpci (Fig. S3B). Consistent with the RNA-seq data (Fig. 5A,B), qPCR and ISH analyses revealed increased expression of *mmp9*, *ctssb.1* and *tnfrsf9a* in regenerating hearts upon Notch inhibition at later stages (Fig. S8E-H). Moreover, an augmented number of wound endocardial cells expressed the pro-inflammatory gene *tnfrsf9a* in hearts after RO treatment, as compared with DMSO-treated hearts (Fig. 5G,H). Notch inhibition further caused elevated numbers of *l-plastin*$^+$ and *mpeg1*$^+$ macrophages associated with wound endocardial cells (Fig. 5I-K, Fig. S8I), and an increased abundance of *l-plastin*$^+$ macrophages could be detected until 30 dpci after long-term Notch inhibition (Fig. 5L). These observations suggest that Notch

Development (2017) 144, 1425-1440 doi:10.1242/dev.143362

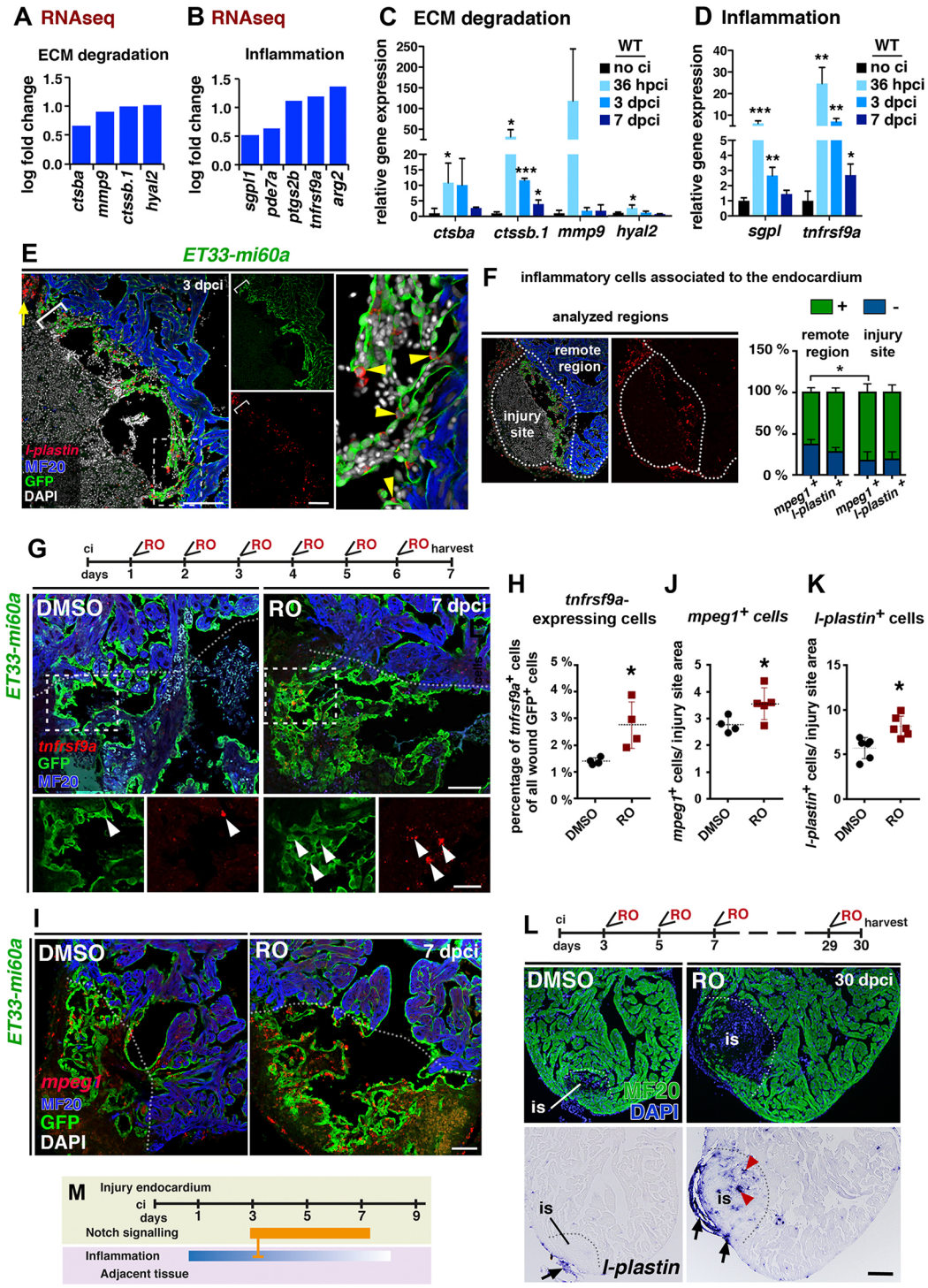

Fig. 5. Notch signalling inhibition affects inflammatory gene expression and macrophage abundance. (A,B) RNA-seq analysis. Differential cardiac expression of genes related to ECM remodelling (A) and inflammation (B) in RO-treated fish at 3 dpci. (C,D) qPCR analysis of hearts with no cryoinjury (no ci) and at indicated time points following cryoinjury. Mean±s.d.; *t*-test, **P*<0.05, ***P*<0.01, ****P*<0.005. (E) FISH combined with IHC, showing *l-plastin*$^+$ cells (arrowheads) in contact with GFP$^+$ cells. *l-plastin*$^+$ cell accumulations at the injury site locally coincide with high endocardial cell abundance (brackets). (F) The percentage of *mpeg1*-expressing or *l-plastin*-expressing inflammatory cells that contact (green) or do not contact (blue) endocardial cells at the injury site or remote region. Inflammatory cells at the outer epicardial region were not considered. (G) *tnfrsf9a* FISH combined with IHC. RO-treated hearts (regime indicated at top) show more GFP$^+$ cells expressing *tnfrsf9a*. (H) Scatter plot showing percentage of *tnfrsf9a*$^+$ endocardial cells. Mean±s.d.; *t*-test, **P*<0.05. (I) *mpeg1* FISH combined with IHC. RO treatment (regime in G) increased *mpeg1*$^+$ macrophage abundance associated with the GFP$^+$ endocardium. (J,K) Scatter plots of the number of *mpeg1*$^+$ (J) or *l-plastin*$^+$ (K) macrophages related to the area occupied by GFP$^+$ cells. Only macrophages contacting GFP$^+$ endocardial cells were considered. Mean±s.d.; *t*-test, **P*<0.05. (L) MF20 IHC and *l-plastin* ISH on consecutive heart sections. RO treatment increased the numbers of *l-plastin*$^+$ macrophages inside the MF20$^-$ injury site (red arrowheads). *l-plastin*$^+$ macrophages in the outer region of the injury can be seen in both conditions (arrows). (M) Schematic showing time and intensity of the inflammatory response and Notch signalling activation at the injury site. Dotted lines delineate the injury site (is). Scale bars: 100 µm, except 50 µm in magnified views.

Development (2017) 144, 1425-1440 doi:10.1242/dev.143362

is required to restrict the inflammatory response in the injury site (Fig. 5M).

Notch signalling regulates cardiomyocyte proliferation and differentiation

We observed that endocardial activation and proliferation preceded myocardial regeneration (Fig. 1H-N). High-magnification 3D analysis showed that clusters of injury-adjacent cardiomyocytes were embedded in a dense endocardial network (Fig. 6A), and that myocardial cell protrusions, which are characteristic of migrating cardiomyocytes (Morikawa et al., 2015), were in close contact with endocardial cells (Fig. 6B). To investigate myocardial and endocardial interactions we analysed BrdU incorporation in Myocyte enhancer factor 2 $(Mef2)^{+}$ wound-adjacent cardiomyocytes after Notch signalling manipulation at 7 dpci. Notch inhibition decreased cardiomyocyte proliferation (Fig. S9A,B), consistent with results obtained after ventricular resection (Zhao et al., 2014). Further, we observed that sustained Notch overactivation augmented cardiomyocyte proliferation (Fig. 6C,D), which differs from previous findings (Zhao et al., 2014). Analysis of $Mef2^{+}$ cardiomyocyte density adjacent to the injury site at 7 dpci revealed higher cardiomyocyte numbers in *Tg(UAS:NICD)* than in control hearts (Fig. 6E,F), suggesting that cardiomyocytes accumulate in this region after Notch overactivation.

ISH against *hand2* and *nkx2.5*, hallmark transcription factors of dedifferentiated cardiomyocytes (Lepilina et al., 2006; Fig. S9C), indicated an expansion of dedifferentiated cardiomyocytes in *Tg(UAS:NICD)* hearts (Fig. 6G, Fig. S9D).

We next analysed myocardial genes that were differentially expressed in the RNA-seq, including the immediate early cardiac growth genes *mycb* and *fosab* (Fig. 6H). RNA-seq and ISH data showed that Notch inhibition decreased *mycb* levels in injury-adjacent cardiomyocytes (Fig. 6I), similarly to *fosab* expression (Fig. 6J). Both genes were shown to be expressed in dedifferentiated, proliferating cardiomyocytes in fish (Aguirre et al., 2014; Beauchemin et al., 2015), suggesting that changes in *mycb* and *fosab* expression might be associated with the reduction in cardiomyocyte proliferation in Notch-abrogated hearts. RNA-seq analysis indicated an upregulation of genes encoding sarcomere assembly and function proteins (Fig. 6H). During regeneration, dedifferentiating zebrafish and mouse cardiomyocytes disassemble the sarcomere for cell division to proceed (Jopling et al., 2010; Porrello et al., 2011), and high levels of sarcomeric proteins are characteristic of differentiated cardiomyocytes (O'Meara et al., 2015). Confirming the RNA-seq data, we detected fewer wound-adjacent cardiomyocytes showing decreased levels of *myosin light chain kinase 3* (*mylk3*), which regulates sarcomere assembly (Seguchi et al., 2007), in hearts after RO treatment than in DMSO-treated hearts (Fig. 6K,L). Further, Notch overactivation decreased *tcap* expression in *Tg(UAS:NICD)* transgenic hearts (Fig. 6M). These results suggest that Notch signalling modulations interfere with sarcomeric gene expression and affect cardiomyocyte dedifferentiation.

The early endocardial gene *serpine1* is implicated in endocardial and myocardial proliferation

To identify a potential early endocardial factor, the downregulation of which may depend on Notch signalling at later stages (Fig. 4D), we focused on *plasminogen activator inhibitor 1* (*serpine1*). Secreted Serpine1 is the main physiological inhibitor of urokinase plasminogen activator (uPA) and tissue plasminogen activator (tPA), and thus inhibits fibrinolysis (Declerck and Gils, 2013). Moreover, Serpine1 regulates endothelial cell proliferation (Ploplis et al., 2004), apoptosis (Balsara and Ploplis, 2008; Abderrahmani et al., 2012) and migration (Isogai et al., 2001) and is upregulated in the injured neonatal heart (Darehzereshki et al., 2015).

serpine1 expression was absent in the uninjured adult heart (Fig. S10A) but strongly upregulated early after cryoinjury (36 hpci, 3 dpci, Fig. 7A) and decreased at later stages (Fig. 7A, Fig. S10B). FISH combined with antibody staining detected a high number of *serpine1*-expressing GFP^{+} wound and wound-adjacent endocardial cells (Fig. 7C,D, Fig. S10C) in *ET33-mi60a* fish at 24 hpci and 36 hpci (36.7±6.6% and 35.5±6.8%, respectively). The percentage of *serpine1*-expressing endocardial cells dramatically decreased at 3 dpci (14.4±5.6%; Fig. 7C,D) and remained low at 7 dpci (4.7±0.9%; Fig. 7C,D). Notch inhibition increased *serpine1* expression levels (Fig. 7B, Fig. S10D) and indeed augmented the number of endocardial cells expressing *serpine1* (Fig. 7E,F), indicating that *serpine1* downregulation in the injury site endocardium requires Notch signalling at later stages of regeneration.

To investigate if this regulation could be a common mechanism in endothelial/endocardial cells we treated porcine aortic valve endothelial cells (PAVECs) with RO for 48 h. *SERPINE1* expression was increased in Notch-abrogated PAVECs (Fig. 7G) in parallel with a marked downregulation of Notch targets (not shown). Also, RNA-seq data obtained in various mouse mutants with disrupted endocardial Notch signalling at different time points of development (Luxán et al., 2013; D'Amato et al., 2016) showed significantly increased *Serpine1* expression (Fig. 7G), indicating that, similar to the zebrafish situation (Fig. 7B,E-G), *Serpine1* expression is upregulated in mouse after Notch abrogation.

To investigate the function of Serpine1 in the cryoinjured endocardium, we treated fish with the inhibitor Tiplaxtinin (PAI-039, abbreviated as TP) (Fig. 7H), which blocks Serpine1 protease activity (Gorlatova et al., 2007; Daniel et al., 2015). TP treatment did not interfere with fibrotic tissue deposition (Fig. S10E-G) or endocardial activation, as indicated by the expression of *aldh1a2* (Fig. S10H). However, we detected an augmented number of wound endocardial cells expressing Pcna after TP treatment for 3 dpci (Fig. 7H,I), suggesting that endocardial proliferation at 3 dpci is linked to *serpine1* downregulation in endocardial cells. Also, relative levels of *cdh5* in wound endocardial cells were significantly higher (1.4±0.1; Fig. 7J,K) in TP-treated *ET33-mi60a* fish than in DMSO-treated controls (1.3±0.1; Fig. 7J,K) at 3 dpci, indicating that endocardial maturation had progressed further.

As Serpine1 is a secreted molecule, endocardial Serpine1 might also have non-cell-autonomous functions during heart regeneration. We examined the consequences of TP treatment on cardiomyocyte proliferation, and observed higher numbers of $Pcna^{+}$ cardiomyocytes in TP-treated hearts (Fig. 7L,M), indicating that early Serpine1 abrogation augments cardiomyocyte proliferation. We next treated fish with TP or DMSO during the first days of regeneration (10 dpci), the time frame when we expected *serpine1* expression to be active in the endocardium. Examination of TP- or DMSO-treated injured hearts at 22 dpci did not reveal any difference in injury site size (Fig. 7N,O), suggesting that early Serpine1 inhibition does not result in accelerated regeneration or in interference with collagen deposition or degradation.

In summary, these results reveal *serpine1* as an early endocardial injury-response gene, the downregulation of which at later stages depends on Notch signalling. Moreover, Serpine1 is involved in the regulation of endocardium proliferation and maturation, and non-cell-autonomously influences myocardial proliferation.

Development (2017) 144, 1425-1440 doi:10.1242/dev.143362

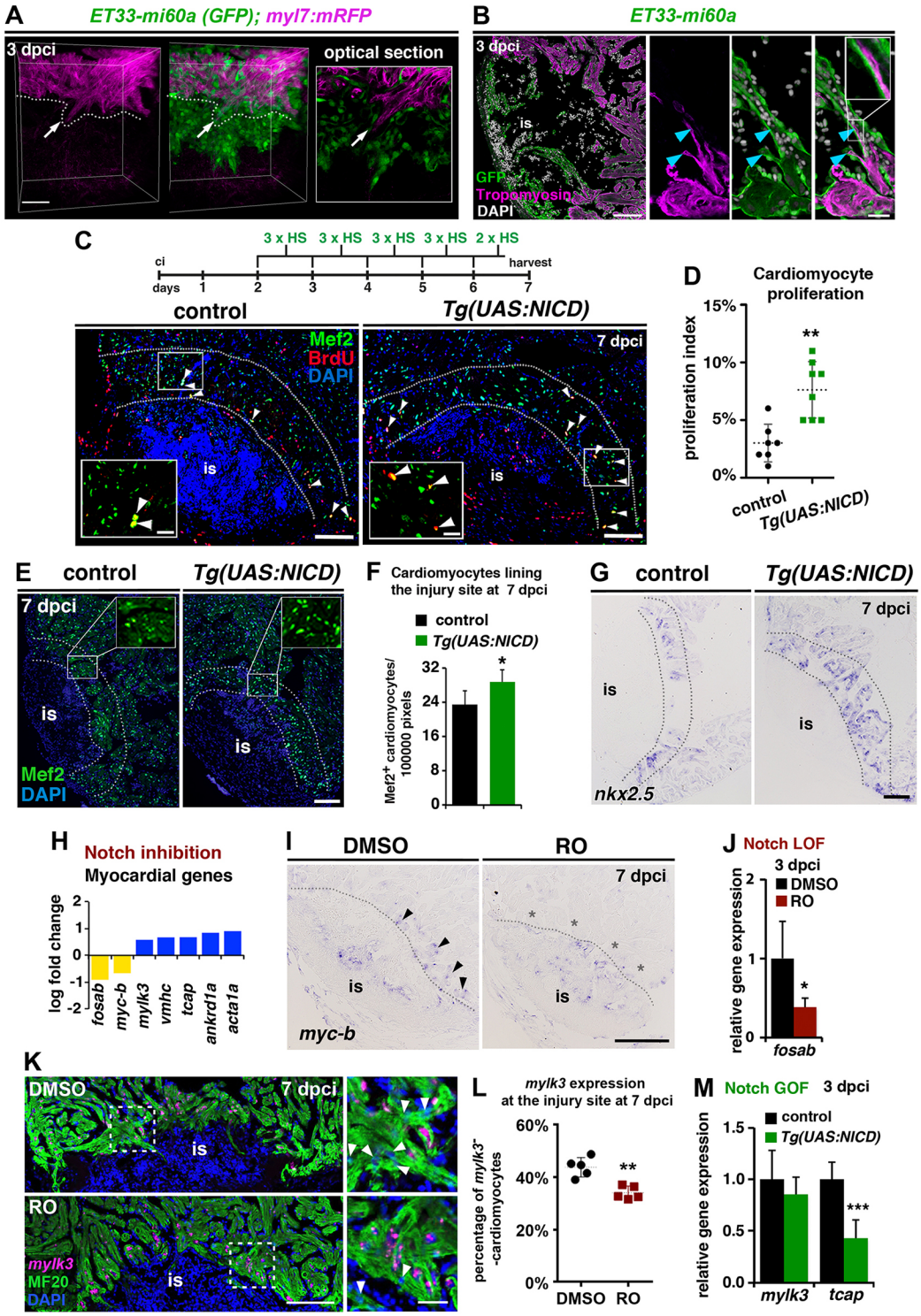

Fig. 6. Notch signalling regulates cardiomyocyte proliferation. (A) *ET33-mi60a;myl7:mRFP* ventricle, volume rendering and optical section of a region of the inner injury border. Endocardial cells surround injury-adjacent cardiomyocytes (arrows) and precede into the wound. (B) IHC showing endocardial cells (GFP$^+$) in contact with myocardial protrusions (tropomyosin$^+$; blue arrowheads). (C,D) IHC against BrdU and Mef2 (C). Heat shock regime is indicated at the top. Scatter plot (D) of percentage of BrdU$^+$ wound-adjacent cardiomyocytes (Mef2$^+$; arrowheads between dotted lines). Mean±s.d.; *t*-test, $^{**}P<0.01$. (E,F) Mef2 IHC showing a higher density of wound-adjacent cardiomyocytes (between the dotted lines) in *Tg(UAS:NICD)* than in control hearts (E), as quantified in F. Mean±s.d.; *t*-test, $^{*}P<0.05$. (G) ISH showing higher numbers of *nkx2.5*$^+$ wound-adjacent cardiomyocytes (between dotted lines) in *Tg(UAS:NICD)* hearts. (H) RNA-seq data showing differential myocardial gene expression in RO-treated hearts at 3 dpci. (I) ISH showing *mycb* expression in injury-adjacent cardiomyocytes (arrowheads) in DMSO-treated but not in RO-treated hearts (asterisks). (J) qPCR levels of *fosab* in the injured heart. Mean±s.d.; *t*-test, $^{*}P<0.05$. LOF, loss of function. (K) MF20 IHC and *mylk3* ISH on heart sections. RO treatment decreased the numbers of *mylk3*$^-$ cardiomyocytes adjacent to the injury site (arrowheads). (L) Scatter plot showing the percentage of *mylk3*$^-$ wound-adjacent (50 µm) cardiomyocytes. Mean±s.d.; *t*-test, $^{**}P<0.01$. (M) qPCR analysis of *mylk3* and *tcap* levels in the injured heart. Mean±s.d.; *t*-test, $^{***}P<0.001$. GOF, gain of function. Dotted lines delineate the injury site (is). Boxed areas are magnified in insets. Scale bars: 100 µm, except 25 µm in magnified views.

Development (2017) 144, 1425-1440 doi:10.1242/dev.143362

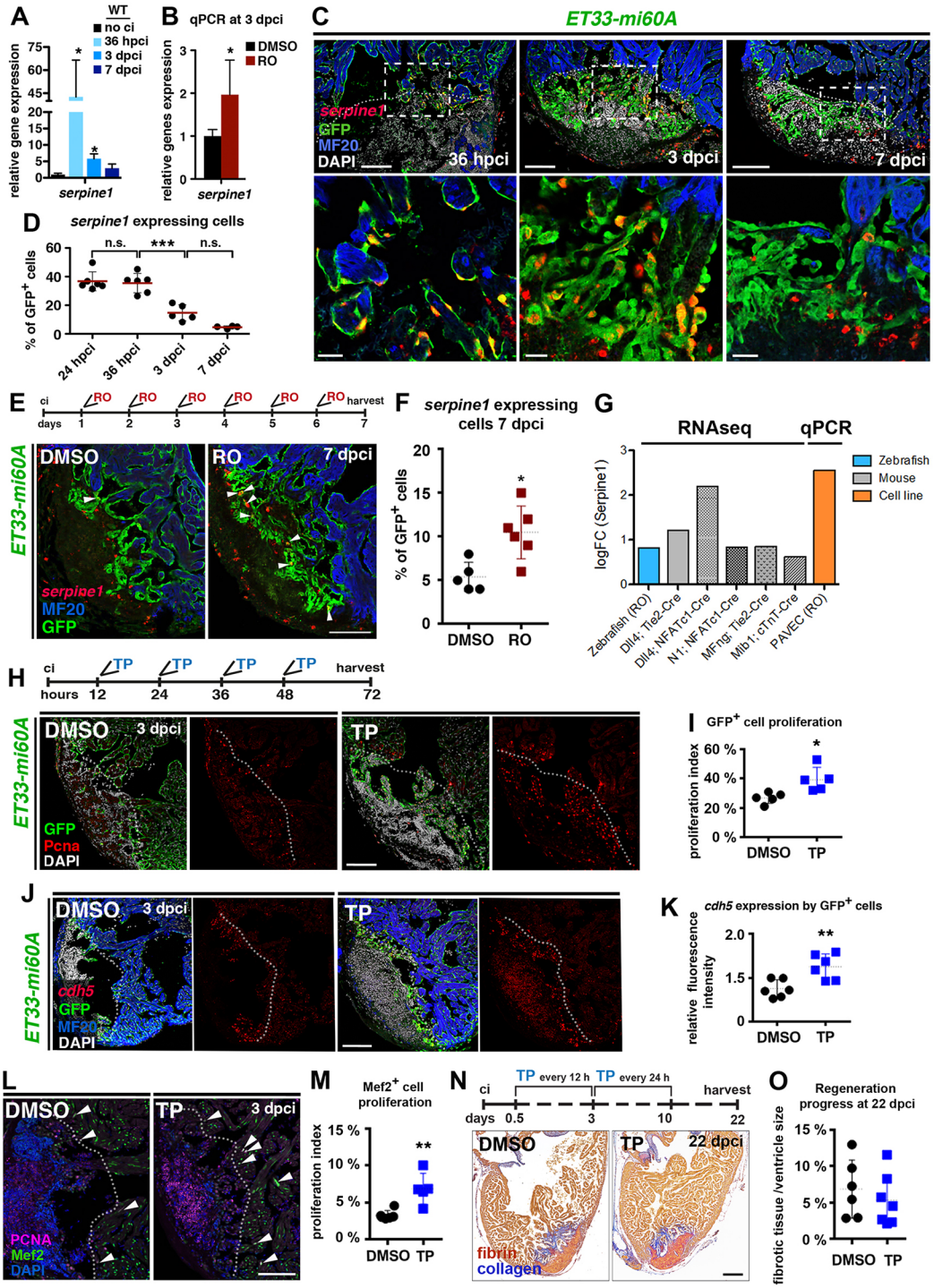

Fig. 7. *serpine1* is upregulated early upon cryoinjury and responds to Notch in endocardial/endothelial cells. (A) qPCR analysis of *serpine1* in hearts with no cryoinjury (no ci) and at indicated time points following cryoinjury. Mean±s.d.; *t*-test, **P*<0.05. (B) *serpine1* qPCR in the injured heart. Mean±s.d.; *t*-test, **P*<0.05. (C) *serpine1* FISH plus IHC. At 36 hpci, numerous wound and wound-adjacent GFP$^+$ endocardial cells express *serpine1*. At 3 and 7 dpci, *serpine1*-expressing wound endocardial cells are less frequent. Boxed areas are magnified beneath. (D) Scatter plot of the percentage of *serpine1*$^+$ cells among all wound and wound-adjacent (50 µm) GFP$^+$ cells. Mean±s.d.; one-way ANOVA and Newman-Keuls test, ****P*<0.005 (see Table S5). (E) *serpine1* FISH combined with IHC. RO-treated hearts (regime indicated at top) show more GPF$^+$ cells expressing *serpine1* (arrowheads). (F) Scatter plot indicating the percentage of *serpine1*$^+$ endocardial cells. Mean±s.d.; *t*-test, **P*<0.05. (G) Log fold change (FC) of *serpine1* showing increased expression as assessed by qPCR in RO-treated PAVECs, by RNA-seq in RO-treated zebrafish hearts and in various murine models of endocardial Notch disruption. (H) IF indicating Pcna$^+$ and GFP$^+$ cells after TP treatment (regime indicated at top). (I) Scatter plot of the relative number of Pcna$^+$ cells among all wound and wound-adjacent GFP$^+$ cells. Mean±s.d.; *t*-test, **P*<0.05. (J) FISH combined with IHC showing that TP treatment increases *cdh5* mRNA levels in GFP$^+$ wound endocardium. (K) Scatter plot of relative red fluorescence intensity, comparing values of remote and wound endocardium (see Fig. 2F). Mean±s.d.; *t*-test, ***P*<0.01. (L) IF revealed more Pcna$^+$ Mef2$^+$ wound-adjacent cardiomyocytes (arrowheads) after TP treatment. (M) Scatter plot of the relative number of Pcna$^+$ cells among all wound-adjacent (100 µm) Mef2$^+$ cardiomyocytes. Mean±s.d.; *t*-test, ***P*<0.01. (N) AFOG-stained hearts, treated with DMSO or TP (treatment regime indicated at top). (O) Scatter plot indicating injury site size (mean±s.d.). Dotted lines delineate injury site. Scale bars: 100 µm in C,E,H,J,L; 200 µm in N; 20 µm in magnified views.

Development (2017) 144, 1425-1440 doi:10.1242/dev.143362

DISCUSSION

Endocardial dynamics at the injury site

In this report we provide the first 3D image analysis of the whole injured region of the zebrafish heart, and describe the dynamics and possible functions of the injured endocardium. Previous studies have reported morphological changes and the activation of wound-adjacent endocardial cells following ventricular resection (Kikuchi et al., 2011). Our results, using the cryoinjury model, reveal a highly dynamic endocardium during the first days of regeneration, with changes in endocardial cell morphology, behaviour and gene expression occurring at distinct phases of regeneration (Fig. 8).

Signals controlling endocardial dynamics

We identified Serpine1 as an early injury-induced molecule in the damaged endocardium (Fig. 8). Despite its inhibitory role in fibrinolysis (Declerck and Gils, 2013), Serpine1 inhibition did not interfere with fibrotic tissue deposition or resolution. We describe one function for Serpine1 as a negative regulator of proliferation and of *cdh5* levels in wound endocardial cells (Fig. 8B). This could imply the involvement of Serpine1 in the maintenance of an initial activation state of the wound endocardium and is in line with its cell-autonomous role in endothelial cells, regulating proliferation or apoptosis (Bajou et al., 2008). Further, we identify Notch as an important player during wound endocardium maturation (Fig. 8), with similar functions in development and regeneration. This holds true for the augmented expression of the developmental genes *heg* and *klf2a* and the increased number of filopodia-presenting wound endocardial cells in Notch-inhibited hearts. During developmental angiogenesis, Notch blocks the migratory tip-cell fate of endothelial cells (Hellström et al., 2007; Lobov et al., 2007; Suchting et al., 2007) and Notch inhibition interferes with blood vessel maturation (Ehling et al., 2013).

Implication of endocardial signals in the inflammatory response and cardiomyocyte proliferation

We observed that early activated endocardium coincides with a high abundance of inflammatory cells and inflammatory gene expression. This raises the hypothesis that endocardial signals may regulate regenerative processes, and that endocardial maturation might be crucial for cardiac regeneration to progress from the inflammatory to the reparative phase (Chablais and Jazwinska, 2012a). During inflammation, vascular endothelial cells mediate the recruitment, adherence and passage of inflammatory cells (Pober and Sessa, 2007). The endocardium might possess this role in the regenerating heart as it responds to inflammatory signals (Kikuchi et al., 2011) and expresses cytokines (Fang et al., 2013). We extend these studies, showing that inflammatory macrophages are associated with wound endocardium. Also, Notch signalling abrogation resulted in increased wound-related endothelial and inflammatory gene expression and an increased abundance of macrophages. This anti-inflammatory role of Notch might be direct, by regulating endothelial inflammatory genes such as *tnfrsf9a* (Olofsson et al., 2008; Teijeira et al., 2012), or might be linked to the appearance and maturation of the endocardium upon Notch inhibition.

Cardiac injury induces the dedifferentiation and proliferation of existing cardiomyocytes, which peaks at 7 dpci (Kikuchi et al., 2010; Sallin et al., 2014; Bednarek et al., 2015), and endocardial signals are implicated in this process (Kikuchi et al., 2011; Zhao et al., 2014). Our results show that endocardial proliferation and

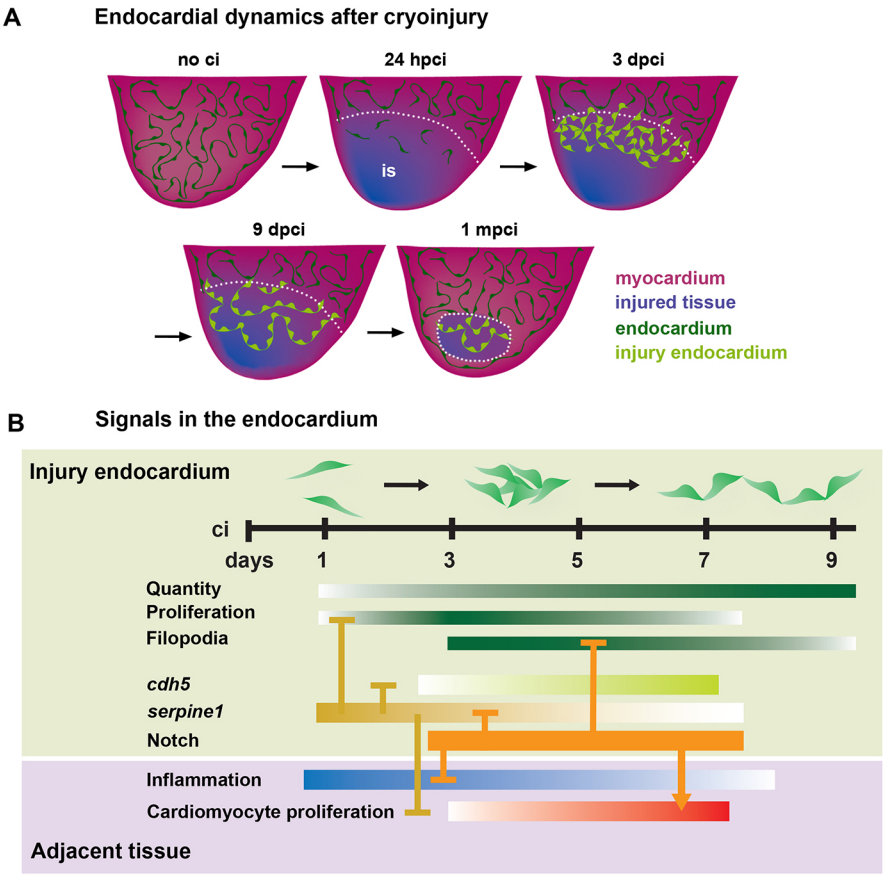

Fig. 8. Endocardial dynamics and signalling after cryoinjury. (A) The tip of the adult zebrafish ventricle in the uninjured situation (no ci), and at various time points after cryoinjury. Uninjured endocardium is depicted as a dark green monolayer and the myocardium in pink; the damaged tissue of the injury site (is) in purple and delineated by a dotted line, with the endocardium colonising the injury site in light green. (B) Injury endocardium is characterised by changes in morphology (filopodia, organisation), behaviour (proliferation, migration) and gene expression (*cdh5*, *serpine1*) at different time points of regeneration. Alterations in endocardial signals (Notch, Serpine1) affect these characteristics (arrows, lines) and interfere with inflammation attenuation (blue) and cardiomyocyte proliferation (red).

Development (2017) 144, 1425-1440 doi:10.1242/dev.143362

regeneration precede the regenerating myocardium. In addition, we revealed a possible non-cell-autonomous effect of Serpine1 and Notch signalling on cardiomyocyte proliferation. Secreted Serpine1 might directly signal to cardiomyocytes, preventing proliferative signals or controlling the degradation of specific ECM components, which are crucial for myocardial proliferation and regeneration (Trinh and Stainier, 2004; Mercer et al., 2013; Wang et al., 2013). The inverse correlation between high endocardial *serpine1* expression and high cardiomyocyte proliferation (Kikuchi et al., 2010; Sallin et al., 2014; Bednarek et al., 2015) (Fig. 8B) at different stages of heart regeneration supports the hypothesis that *serpine1* downregulation is one prerequisite for myocardial proliferation. Moreover, hearts with abrogated Notch signalling, where cardiomyocyte proliferation was decreased, also showed increased levels of *serpine1*. These observations suggest a Notch-mediated downregulation of *serpine1* to regulate cardiomyocyte proliferation. Serpine1 expression is also upregulated in endocardial cells in the cryoinjured mouse heart (Darehzereshki et al., 2015) and might be involved in an evolutionarily conserved mechanism of cardiac repair. The inhibitory relationship between Notch and Serpine1 might be part of this mechanism, as supported by our observation that abrogated Notch signalling caused increased *SERPINE1* expression in endothelial cells (PAVECs) and in mouse embryos. Future studies should investigate the regulatory effect of Notch on *serpine1*, and whether Serpine1 inhibition affects dedifferentiation of cardiomyocytes. Precise regulation of Serpine1 is crucial, as elevated Serpine1 levels increase cardiac fibrosis upon myocardial infarction in mice (Takeshita et al., 2004), whereas *Serpine1* deficiency leads to cardiac fibrosis (Moriwaki et al., 2004).

In our study, Notch overactivation led to increased BrdU incorporation by injury-adjacent cardiomyocytes (Fig. 8). This result appears to conflict with data from Zhao et al. (2014) showing decreased numbers of $Pcna^{+}$ cardiomyocytes upon Notch overactivation. We further observed the accumulation of dedifferentiated cardiomyocytes at the inner injury border, explaining why Notch overactivation impairs regeneration. We suggest two possible explanations. First, the dedifferentiated, proliferating state of cardiomyocytes might prevent their invasion into the injury. Second, cardiomyocytes might fail to enter the injury site due to altered ECM remodelling or endocardial organisation within the injury site. Our Notch inhibition data would support both possibilities, but this issue requires further investigation.

The results presented here reveal a highly dynamic endocardium after cryoinjury, with changes in cell behaviour, morphology and gene expression during regeneration. We identified *serpine1* as an early endocardial injury-response gene and Notch signalling as a player later during regeneration. The maturation of the endocardium and the control of inflammatory cell infiltration require Notch signalling, and our data suggest that the endocardium promotes myocardial regeneration by providing Serpine1-dependent negative and Notch-dependent positive proliferative signals (Fig. 8). These findings demonstrate the importance of the endocardium in the regulation of the injury response and in regeneration upon cardiac insult. Future analysis of the specific endocardial signals orchestrating inflammation, fibrotic tissue deposition and cardiomyocyte renewal could contribute to the development of therapeutic applications for cardiac diseases.

MATERIALS AND METHODS

Zebrafish husbandry

Animal studies were approved by the CNIC Animal Experimentation Ethics Committee and by the Community of Madrid (ref. PROEX 118/15). Animal procedures conformed to EU Directive 2010/63EU and Recommendation 2007/526/EC regarding the protection of animals used for experimental and scientific purposes, enforced in Spanish law under Real Decreto 53/2013. Zebrafish were raised and maintained under standard conditions (Kimmel et al., 1995). Cryoinjury was performed as described (González-Rosa and Mercader, 2012). Details of transgenic lines used are provided in the supplementary Materials and Methods.

Treatments

Adult zebrafish were injected intraperitoneally with 30 µl RO4929097 (S1575, Selleckchem; 600 µM in PBS) or DMSO as a control. Treatment regimens of each experiment are indicated in the corresponding figure. Embryos were incubated in fishwater containing DMSO or RO (50 µM). 30 µl Tiplaxtinin (PAI-039, S7922, Selleckchem; 1500 µM) or DMSO in PBS was injected intraperitoneally following the treatment regime indicated in the figures. See the supplementary Materials and Methods for further details.

Histology

Hearts were fixed in 4% paraformaldehyde (PFA) overnight, dehydrated, embedded in paraffin and sectioned at 7 µm. Serial sections were distributed on several slides, such that each slide contained sections of several levels of the heart. One or two slides of each heart were used for Acid Fuchsin-Orange G (AFOG) staining, immunohistochemistry (IHC) or *in situ* hybridisation (ISH) to obtain stained sections randomly distributed throughout the heart for unbiased quantification (see below). Primers used to generate RNA probes are listed in Table S7. IHC was performed as described (González-Rosa et al., 2011). For IHC on vibratome sections, hearts were fixed in 4% PFA overnight, washed with PBST (0.1% Tween in PBS) and embedded in 4% low melting point agarose. Sections of 70 µm were obtained and kept in PBST. For IHC, sections were incubated in blocking solution (5% BSA, 5% goat serum, PBS) for 1 h and then in primary antibody overnight at 4°C. After extensive washes with PBST, heart sections were incubated overnight with secondary antibody and FITC-coupled phalloidin. Extensive washes and a 30 min incubation with DAPI followed. Sections were mounted in Fluoromount (Sigma) for imaging. For details of antibodies and imaging see the supplementary Materials and Methods.

Cell culture

Isolation of porcine aortic valve endothelial cells (PAVECs) was carried out as described (Gould et al., 2010). Cells at passage five were seeded on gelatin-coated 6-well dishes (2.1×10^5 cells/well) and cultured in Dulbecco's Modified Eagle's Medium (DMEM; Gibco) supplemented with fetal bovine serum (FBS; 10%), penicillin-streptomycin (1%) and bovine brain extract (20 ng/ml). After 24 h incubation, cells near confluence were serum starved (with 0.5% FBS) and treated with 10 µM RO or vehicle (DMSO) for 12, 36 or 48 h. After the corresponding incubation periods, cells were washed twice with PBS and collected for RNA extraction. Each time point was conducted in triplicate.

Gene expression analysis

For quantitative PCR (qPCR) and RNA sequencing (RNA-seq), hearts were dissected at different time points and apical portions of the three ventricles were pooled and (Fig. 4A) used for RNA extraction using Direct-zol RNA MiniPrep (Zymo Research). cDNA was synthesized with the SuperScript III First Strand Kit (Invitrogen). For qRT-PCR, three hearts were pooled, and the data represented here are from four to six samples. Primer sequences are provided in Tables S8 and S9. See the supplementary Materials and Methods for further details. For RNA-seq analysis, we used three pools, each of three apexes from RO- or DMSO-treated fish. cDNA libraries were prepared with a TruSeq RNA Sample Preparation Kit v2 (Illumina) and were sequenced in a Genome Analyzer IIx Illumina sequencer using a 75 bp single-end elongation protocol. Sequenced reads were quality controlled and pre-processed using Cutadapt v1.6 to remove adaptor contaminants (Martin, 2011). The resulting reads were aligned and gene expression was quantified with RSEM v1.2.3 (Li and Dewey, 2011), using the Zv9_75

zebrafish reference genome. Differentially expressed genes were defined as those with altered expression levels with an adjusted $P<0.05$. RNA-seq data were analysed using Ingenuity Pathway Analysis Software (QIAGEN Bioinformatics).

Quantification and statistical analysis

For details of quantification and statistical analysis, including 3D volume, filopodia-like protrusions, fibrotic tissue, IF or ISH staining, BrdU incorporation, macrophage numbers and cardiomyocyte density, see the supplementary Materials and Methods. Sample numbers for all data are listed in Tables S1 and S2.

Acknowledgements

We thank E. Díaz for husbandry; B. Rios, V. Bou, R. Doohan, P. Martínez for technical help; the CNIC Microscopy Unit for advice; F. Sánchez-Cabo for help with statistics; and S. Bartlett and K. McCreath for English editing. RNA-seq and bioinformatics analysis were performed by the CNIC Genomics and Bioinformatics Units. The *Tg(hsp70l:Gal4)^{kca4};Tg(UAS:myc-Notch1a-intra)^{kca3}* line was from N. Lawson and the *ET(krt4:EGFP)$^{sqet33\text{-}mi60a}$* and *ET(krt4:EGFP)$^{sqet33\text{-}1A}$* lines were from V. Korz. We are grateful to A. Oates, G. Weidinger, D. Goldman, S. Sumanas, J. Vermot and A. Kawakami for probes.

Competing interests

The authors declare no competing or financial interests.

Author contributions

J.M., D.G., A.G.-R., R.T.-C. performed experiments. J.M. and J.L.d.l.P. designed experiments, reviewed the data and wrote the manuscript. All authors reviewed the manuscript during its preparation.

Funding

This work was supported by grants SAF2013-45543-R, RD12/0042/0005 (RIC), RD12/0019/0003 (TERCEL) and CB16/11/00399 (CIBER CV) from the Spanish Ministry of Economy, Industry and Competitiveness [Ministerio de Economía, Industria y Competitividad (MINECO)]; FP7-ITN 215761 (NotchIT) and PITN-GA-2011-289600 (CardioNeT) from the European Commission to J.L.d.l.P. J.M. held a PhD fellowship linked to grant FP7-ITN 215761 (NotchIT). The cost of this publication has been paid in part with Fonds Européen de Développement Régional (FEDER) funds. The CNIC is supported by MINECO and the Pro-CNIC Foundation, and is a 'Severo Ochoa' Center of Excellence (MINECO award SEV-2015-0505).

Data availability

RNA-seq data are deposited at NCBI Gene Expression Omnibus under accession number GSE68650.

Supplementary information

Supplementary information available online at
http://dev.biologists.org/lookup/doi/10.1242/dev.143362.supplemental

References

Abderrahmani, R., Francois, A., Buard, V., Tarlet, G., Blirando, K., Hneino, M., Vaurijoux, A., Benderitter, M., Sabourin, J.-C. and Milliat, F. (2012). PAI-1-dependent endothelial cell death determines severity of radiation-induced intestinal injury. *PLoS ONE* **7**, e35740.

Aguirre, A., Montserrat, N., Zacchigna, S., Nivet, E., Hishida, T., Krause, M. N., Kurian, L., Ocampo, A., Vazquez-Ferrer, E., Rodriguez-Esteban, C. et al. (2014). In vivo activation of a conserved microRNA program induces mammalian heart regeneration. *Cell Stem Cell* **15**, 589-604.

Bajou, K., Peng, H., Laug, W. E., Maillard, C., Noel, A., Foidart, J. M., Martial, J. A. and DeClerck, Y. A. (2008). Plasminogen activator inhibitor-1 protects endothelial cells from FasL-mediated apoptosis. *Cancer Cell* **14**, 324-334.

Balsara, R. D. and Ploplis, V. A. (2008). Plasminogen activator inhibitor-1: the double-edged sword in apoptosis. *Thromb. Haemostasis* **100**, 1029-1036.

Beauchemin, M., Smith, A. and Yin, V. P. (2015). Dynamic microRNA-101a and Fosab expression controls zebrafish heart regeneration. *Development* **142**, 4026-4037.

Bednarek, D., González-Rosa, J. M., Guzman-Martinez, G., Gutierrez-Gutierrez, O., Aguado, T., Sanchez-Ferrer, C., Marques, I. J., Galardi-Castilla, M., de Diego, I., Gomez, M. J. et al. (2015). Telomerase is essential for zebrafish heart regeneration. *Cell Rep.* **12**, 1691-1703.

Chablais, F. and Jazwinska, A. (2012a). The regenerative capacity of the zebrafish heart is dependent on TGFbeta signaling. *Development* **139**, 1921-1930.

Chablais, F. and Jazwinska, A. (2012b). Induction of myocardial infarction in adult zebrafish using cryoinjury. *J. Vis. Exp.* **62**, pii: 3666.

Chablais, F., Veit, J., Rainer, G. and Jaźwińska, A. (2011). The zebrafish heart regenerates after cryoinjury-induced myocardial infarction. *BMC Dev. Biol.* **11**, 21.

Chowdhury, B., Hemming, R., Hombach-Klonisch, S., Flamion, B. and Triggs-Raine, B. (2013). Murine hyaluronidase 2 deficiency results in extracellular hyaluronan accumulation and severe cardiopulmonary dysfunction. *J. Biol. Chem.* **288**, 520-528.

Conner, C., Ackerman, K. M., Lahne, M., Hobgood, J. S. and Hyde, D. R. (2014). Repressing notch signaling and expressing TNFalpha are sufficient to mimic retinal regeneration by inducing Muller glial proliferation to generate committed progenitor cells. *J. Neurosci.* **34**, 14403-14419.

Conrad, C. H., Brooks, W. W., Hayes, J. A., Sen, S., Robinson, K. G. and Bing, O. H. L. (1995). Myocardial fibrosis and stiffness with hypertrophy and heart failure in the spontaneously hypertensive rat. *Circulation* **91**, 161-170.

D'Amato, G., Luxán, G., del Monte-Nieto, G., Martínez-Poveda, B., Torroja, C., Walter, W., Bochter, M. S., Benedito, R., Cole, S., Martinez, F. et al. (2016). Sequential Notch activation regulates ventricular chamber development. *Nat. Cell Biol.* **18**, 7-20.

Daniel, A. E., Timmerman, I., Kovacevic, I., Hordijk, P. L., Adriaanse, L., Paatero, I., Belting, H.-G. and van Buul, J. D. (2015). Plasminogen activator inhibitor-1 controls vascular integrity by regulating VE-cadherin trafficking. *PLoS ONE* **10**, e0145684.

Darehzereshki, A., Rubin, N., Gamba, L., Kim, J., Fraser, J., Huang, Y., Billings, J., Mohammadzadeh, R., Wood, J., Warburton, D. et al. (2015). Differential regenerative capacity of neonatal mouse hearts after cryoinjury. *Dev. Biol.* **399**, 91-99.

Declerck, P. J. and Gils, A. (2013). Three decades of research on plasminogen activator inhibitor-1: a multifaceted serpin. *Semin. Thromb. Hemost.* **39**, 356-364.

Dekker, R. J., van Soest, S., Fontijn, R. D., Salamanca, S., de Groot, P. G., VanBavel, E., Pannekoek, H. and Horrevoets, A. J. (2002). Prolonged fluid shear stress induces a distinct set of endothelial cell genes, most specifically lung Kruppel-like factor (KLF2). *Blood* **100**, 1689-1698.

Dekker, R. J., Boon, R. A., Rondaij, M. G., Kragt, A., Volger, O. L., Elderkamp, Y. W., Meijers, J. C., Voorberg, J., Pannekoek, H. and Horrevoets, A. J. (2006). KLF2 provokes a gene expression pattern that establishes functional quiescent differentiation of the endothelium. *Blood* **107**, 4354-4363.

Dobaczewski, M., Gonzalez-Quesada, C. and Frangogiannis, N. G. (2010). The extracellular matrix as a modulator of the inflammatory and reparative response following myocardial infarction. *J. Mol. Cell. Cardiol.* **48**, 504-511.

Ehling, M., Adams, S., Benedito, R. and Adams, R. H. (2013). Notch controls retinal blood vessel maturation and quiescence. *Development* **140**, 3051-3061.

Ellett, F., Pase, L., Hayman, J. W., Andrianopoulos, A. and Lieschke, G. J. (2011). mpeg1 promoter transgenes direct macrophage-lineage expression in zebrafish. *Blood* **117**, e49-e56.

Fang, Y., Gupta, V., Karra, R., Holdway, J. E., Kikuchi, K. and Poss, K. D. (2013). Translational profiling of cardiomyocytes identifies an early Jak1/Stat3 injury response required for zebrafish heart regeneration. *Proc. Natl. Acad. Sci. USA* **110**, 13416-13421.

Felician, G., Collesi, C., Lusic, M., Martinelli, V., Ferro, M. D., Zentilin, L., Zacchigna, S. and Giacca, M. (2014). Epigenetic modification at Notch responsive promoters blunts efficacy of inducing notch pathway reactivation after myocardial infarction. *Circ. Res.* **115**, 636-649.

Frangogiannis, N. G. (2008). The immune system and cardiac repair. *Pharmacol. Res.* **58**, 88-111.

Gemberling, M., Bailey, T. J., Hyde, D. R. and Poss, K. D. (2013). The zebrafish as a model for complex tissue regeneration. *Trends Genet.* **29**, 611-620.

González-Rosa, J. M. and Mercader, N. (2012). Cryoinjury as a myocardial infarction model for the study of cardiac regeneration in the zebrafish. *Nat. Protoc.* **7**, 782-788.

González-Rosa, J. M., Martin, V., Peralta, M., Torres, M. and Mercader, N. (2011). Extensive scar formation and regression during heart regeneration after cryoinjury in zebrafish. *Development* **138**, 1663-1674.

Gorlatova, N. V., Cale, J. M., Elokdah, H., Li, D., Fan, K., Warnock, M., Crandall, D. L. and Lawrence, D. A. (2007). Mechanism of inactivation of plasminogen activator inhibitor-1 by a small molecule inhibitor. *J. Biol. Chem.* **282**, 9288-9296.

Gould, R. A. and Butcher, J. T. (2010). Isolation of valvular endothelial cells. *J. Vis. Exp.* **46**, 2158.

Grego-Bessa, J., Luna-Zurita, L., del Monte, G., Bolos, V., Melgar, P., Arandilla, A., Garratt, A. N., Zang, H., Mukouyama, Y.-S., Chen, H. et al. (2007). Notch signaling is essential for ventricular chamber development. *Dev. Cell* **12**, 415-429.

Han, P., Zhou, X.-H., Chang, N., Xiao, C.-L., Yan, S., Ren, H., Yang, X.-Z., Zhang, M.-L., Wu, Q., Tang, B. et al. (2014). Hydrogen peroxide primes heart regeneration with a derepression mechanism. *Cell Res.* **24**, 1091-1107.

Harris, I. S. and Black, B. L. (2010). Development of the endocardium. *Pediatr. Cardiol.* **31**, 391-399.

Hellström, M., Phng, L.-K., Hofmann, J. J., Wallgard, E., Coultas, L., Lindblom, P., Alva, J., Nilsson, A.-K., Karlsson, L., Gaiano, N. et al. (2007). Dll4 signalling

through Notch1 regulates formation of tip cells during angiogenesis. *Nature* **445**, 776-780.
Herbomel, P., Thisse, B. and Thisse, C. (1999). Ontogeny and behaviour of early macrophages in the zebrafish embryo. *Development* **126**, 3735-3745.
Isogai, C., Laug, W. E., Shimada, H., Declerck, P. J., Stins, M. F., Durden, D. L., Erdreich-Epstein, A. and DeClerck, Y. A. (2001). Plasminogen activator inhibitor-1 promotes angiogenesis by stimulating endothelial cell migration toward fibronectin. *Cancer Res.* **61**, 5587-5594.
Itou, J., Oishi, I., Kawakami, H., Glass, T. J., Richter, J., Johnson, A., Lund, T. C. and Kawakami, Y. (2012). Migration of cardiomyocytes is essential for heart regeneration in zebrafish. *Development* **139**, 4133-4142.
Jopling, C., Sleep, E., Raya, M., Martí, M., Raya, A. and Belmonte, J. C. I. (2010). Zebrafish heart regeneration occurs by cardiomyocyte dedifferentiation and proliferation. *Nature* **464**, 606-609.
Kikuchi, K. (2015). Dedifferentiation, transdifferentiation, and proliferation: mechanisms underlying cardiac muscle regeneration in zebrafish. *Curr. Pathobiol. Rep.* **3**, 81-88.
Kikuchi, K., Holdway, J. E., Werdich, A. A., Anderson, R. M., Fang, Y., Egnaczyk, G. F., Evans, T., MacRae, C. A., Stainier, D. Y. R. and Poss, K. D. (2010). Primary contribution to zebrafish heart regeneration by gata4(+) cardiomyocytes. *Nature* **464**, 601-605.
Kikuchi, K., Holdway, J. E., Major, R. J., Blum, N., Dahn, R. D., Begemann, G. and Poss, K. D. (2011). Retinoic acid production by endocardium and epicardium is an injury response essential for zebrafish heart regeneration. *Dev. Cell* **20**, 397-404.
Kimmel, C. B., Ballard, W. W., Kimmel, S. R., Ullmann, B. and Schilling, T. F. (1995). Stages of embryonic development of the zebrafish. *Dev. Dyn.* **203**, 253-310.
Kleaveland, B., Zheng, X., Liu, J. J., Blum, Y., Tung, J. J., Zou, Z., Sweeney, S. M., Chen, M., Guo, L., Lu, M.-M. et al. (2009). Regulation of cardiovascular development and integrity by the heart of glass-cerebral cavernous malformation protein pathway. *Nat. Med.* **15**, 169-176.
Larson, J. D., Wadman, S. A., Chen, E., Kerley, L., Clark, K. J., Eide, M., Lippert, S., Nasevicius, A., Ekker, S. C., Hackett, P. B. et al. (2004). Expression of VE-cadherin in zebrafish embryos: a new tool to evaluate vascular development. *Dev. Dyn.* **231**, 204-213.
Lawson, N. D. and Weinstein, B. M. (2002). In vivo imaging of embryonic vascular development using transgenic zebrafish. *Dev. Biol.* **248**, 307-318.
Lepilina, A., Coon, A. N., Kikuchi, K., Holdway, J. E., Roberts, R. W., Burns, C. G. and Poss, K. D. (2006). A dynamic epicardial injury response supports progenitor cell activity during zebrafish heart regeneration. *Cell* **127**, 607-619.
Li, B. and Dewey, C. N. (2011). RSEM: accurate transcript quantification from RNA-Seq data with or without a reference genome. *BMC Bioinformatics* **12**, 323.
Lobov, I. B., Renard, R. A., Papadopoulos, N., Gale, N. W., Thurston, G., Yancopoulos, G. D. and Wiegand, S. J. (2007). Delta-like ligand 4 (Dll4) is induced by VEGF as a negative regulator of angiogenic sprouting. *Proc. Natl. Acad. Sci. USA* **104**, 3219-3224.
Luxán, G., Casanova, J. C., Martínez-Poveda, B., Prados, B., D'Amato, G., MacGrogan, D., Gonzalez-Rajal, A., Dobarro, D., Torroja, C., Martinez, F. et al. (2013). Mutations in the NOTCH pathway regulator MIB1 cause left ventricular noncompaction cardiomyopathy. *Nat. Med.* **19**, 193-201.
Luxán, G., D'Amato, G., MacGrogan, D. and de la Pompa, J. L. (2016). Endocardial notch signaling in cardiac development and disease. *Circ. Res.* **118**, e1-e18.
Mably, J. D., Mohideen, M. A., Burns, C. G., Chen, J.-N. and Fishman, M. C. (2003). heart of glass regulates the concentric growth of the heart in zebrafish. *Curr. Biol.* **13**, 2138-2147.
Mallavarapu, A. and Mitchison, T. (1999). Regulated actin cytoskeleton assembly at filopodium tips controls their extension and retraction. *J. Cell Biol.* **146**, 1097-1106.
Martin, M. (2011). Cutadapt removes adapter sequences from high-throughput sequencing reads. *EMBnet. J.* **17**, 10-12.
Mattila, P. K. and Lappalainen, P. (2008). Filopodia: molecular architecture and cellular functions. *Nat. Rev. Mol. Cell Biol.* **9**, 446-454.
Mercer, S. E., Odelberg, S. J. and Simon, H.-G. (2013). A dynamic spatiotemporal extracellular matrix facilitates epicardial-mediated vertebrate heart regeneration. *Dev. Biol.* **382**, 457-469.
Mitchell, I. C., Brown, T. S., Terada, L. S., Amatruda, J. F. and Nwariaku, F. E. (2010). Effect of vascular cadherin knockdown on zebrafish vasculature during development. *PLoS ONE* **5**, e8807.
Morikawa, Y., Zhang, M., Heallen, T., Leach, J., Tao, G., Xiao, Y., Bai, Y., Li, W., Willerson, J. T. and Martin, J. F. (2015). Actin cytoskeletal remodeling with protrusion formation is essential for heart regeneration in Hippo-deficient mice. *Sci. Signal.* **8**, ra41.
Moriwaki, H., Stempien-Otero, A., Kremen, M., Cozen, A. E. and Dichek, D. A. (2004). Overexpression of urokinase by macrophages or deficiency of plasminogen activator inhibitor type 1 causes cardiac fibrosis in mice. *Circ. Res.* **95**, 637-644.
Munch, J., Gonzalez-Rajal, A. and de la Pompa, J. L. (2013). Notch regulates blastema proliferation and prevents differentiation during adult zebrafish fin regeneration. *Development* **140**, 1402-1411.
Nemir, M., Metrich, M., Plaisance, I., Lepore, M., Cruchet, S., Berthonneche, C., Sarre, A., Radtke, F. and Pedrazzini, T. (2014). The Notch pathway controls fibrotic and regenerative repair in the adult heart. *Eur. Heart J.* **35**, 2174-2185.
Ogryzko, N. V., Hoggett, E. E., Solaymani-Kohal, S., Tazzyman, S., Chico, T. J. A., Renshaw, S. A. and Wilson, H. L. (2014). Zebrafish tissue injury causes upregulation of interleukin-1 and caspase-dependent amplification of the inflammatory response. *Dis. Model. Mech.* **7**, 259-264.
Olofsson, P. S., Soderstrom, L. A., Wagsater, D., Sheikine, Y., Ocaya, P., Lang, F., Rabu, C., Chen, L., Rudling, M., Aukrust, P. et al. (2008). CD137 is expressed in human atherosclerosis and promotes development of plaque inflammation in hypercholesterolemic mice. *Circulation* **117**, 1292-1301.
O'Meara, C. C., Wamstad, J. A., Gladstone, R. A., Fomovsky, G. M., Butty, V. L., Shrikumar, A., Gannon, J. B., Boyer, L. A. and Lee, R. T. (2015). Transcriptional reversion of cardiac myocyte fate during Mammalian cardiac regeneration. *Circ. Res.* **116**, 804-815.
Ploplis, V. A., Balsara, R., Sandoval-Cooper, M. J., Yin, Z. J., Batten, J., Modi, N., Gadoua, D., Donahue, D., Martin, J. A. and Castellino, F. J. (2004). Enhanced in vitro proliferation of aortic endothelial cells from plasminogen activator inhibitor-1-deficient mice. *J. Biol. Chem.* **279**, 6143-6151.
Pober, J. S. and Sessa, W. C. (2007). Evolving functions of endothelial cells in inflammation. *Nat. Rev. Immunol.* **7**, 803-815.
Poon, K.-L., Liebling, M., Kondrychyn, I., Garcia-Lecea, M. and Korzh, V. (2010). Zebrafish cardiac enhancer trap lines: new tools for in vivo studies of cardiovascular development and disease. *Dev. Dyn.* **239**, 914-926.
Porrello, E. R., Mahmoud, A. I., Simpson, E., Hill, J. A., Richardson, J. A., Olson, E. N. and Sadek, H. A. (2011). Transient regenerative potential of the neonatal mouse heart. *Science* **331**, 1078-1080.
Raya, A., Koth, C. M., Buscher, D., Kawakami, Y., Itoh, T., Raya, R. M., Sternik, G., Tsai, H.-J., Rodriguez-Esteban, C. and Izpisua-Belmonte, J. C. (2003). Activation of Notch signaling pathway precedes heart regeneration in zebrafish. *Proc. Natl. Acad. Sci. USA* **100** Suppl. 1, 11889-11895.
Ridley, A. J. (2011). Life at the leading edge. *Cell* **145**, 1012-1022.
Rohr, S., Otten, C. and Abdelilah-Seyfried, S. (2008). Asymmetric involution of the myocardial field drives heart tube formation in zebrafish. *Circ. Res.* **102**, e12-e19.
Ryoo, S., Gupta, G., Benjo, A., Lim, H. K., Camara, A., Sikka, G., Lim, H. K., Sohi, J., Santhanam, L., Soucy, K. et al. (2008). Endothelial arginase II: a novel target for the treatment of atherosclerosis. *Circ. Res.* **102**, 923-932.
Sallin, P., de Preux Charles, A. S., Duruz, V., Pfefferli, C. and Jazwinska, A. (2014). A dual epimorphic and compensatory mode of heart regeneration in zebrafish. *Dev. Biol.* **399**, 27-40.
Scheer, N., Groth, A., Hans, S. and Campos-Ortega, J. A. (2001). An instructive function for Notch in promoting gliogenesis in the zebrafish retina. *Development* **128**, 1099-1107.
Schnabel, K., Wu, C.-C., Kurth, T. and Weidinger, G. (2011). Regeneration of cryoinjury induced necrotic heart lesions in zebrafish is associated with epicardial activation and cardiomyocyte proliferation. *PLoS ONE* **6**, e18503.
Seguchi, O., Takashima, S., Yamazaki, S., Asakura, M., Asano, Y., Shintani, Y., Wakeno, M., Minamino, T., Kondo, H., Furukawa, H. et al. (2007). A cardiac myosin light chain kinase regulates sarcomere assembly in the vertebrate heart. *J. Clin. Invest.* **117**, 2812-2824.
Smith, S. J., Brookes-Fazakerley, S., Donnelly, L. E., Barnes, P. J., Barnette, M. S. and Giembycz, M. A. (2003). Ubiquitous expression of phosphodiesterase 7A in human proinflammatory and immune cells. *Am. J. Physiol. Lung Cell. Mol. Physiol.* **284**, L279-L289.
Suchting, S., Freitas, C., le Noble, F., Benedito, R., Breant, C., Duarte, A. and Eichmann, A. (2007). The Notch ligand Delta-like 4 negatively regulates endothelial tip cell formation and vessel branching. *Proc. Natl. Acad. Sci. USA* **104**, 3225-3230.
Susaki, E. A., Tainaka, K., Perrin, D., Kishino, F., Tawara, T., Watanabe, T. M., Yokoyama, C., Onoe, H., Eguchi, M., Yamaguchi, S. et al. (2014). Whole-brain imaging with single-cell resolution using chemical cocktails and computational analysis. *Cell* **157**, 726-739.
Takeshita, K., Hayashi, M., Iino, S., Kondo, T., Inden, Y., Iwase, M., Kojima, T., Hirai, M., Ito, M., Loskutoff, D. J. et al. (2004). Increased expression of plasminogen activator inhibitor-1 in cardiomyocytes contributes to cardiac fibrosis after myocardial infarction. *Am. J. Pathol.* **164**, 449-456.
Teijeira, A., Palazon, A., Garasa, S., Marre, D., Auba, C., Rogel, A., Murillo, O., Martinez-Forero, I., Lang, F., Melero, I. et al. (2012). CD137 on inflamed lymphatic endothelial cells enhances CCL21-guided migration of dendritic cells. *FASEB J.* **26**, 3380-3392.
Trinh, L. A. and Stainier, D. Y. R. (2004). Fibronectin regulates epithelial organization during myocardial migration in zebrafish. *Dev. Cell* **6**, 371-382.
Vermot, J., Forouhar, A. S., Liebling, M., Wu, D., Plummer, D., Gharib, M. and Fraser, S. E. (2009). Reversing blood flows act through klf2a to ensure normal valvulogenesis in the developing heart. *PLoS Biol.* **7**, e1000246.

Development (2017) 144, 1425-1440 doi:10.1242/dev.143362

Wang, J., Panakova, D., Kikuchi, K., Holdway, J. E., Gemberling, M., Burris, J. S., Singh, S. P., Dickson, A. L., Lin, Y.-F., Sabeh, M. K. et al. (2011). The regenerative capacity of zebrafish reverses cardiac failure caused by genetic cardiomyocyte depletion. *Development* **138**, 3421-3430.

Wang, J., Karra, R., Dickson, A. L. and Poss, K. D. (2013). Fibronectin is deposited by injury-activated epicardial cells and is necessary for zebrafish heart regeneration. *Dev. Biol.* **382**, 427-435.

Wong, K. S., Rehn, K., Palencia-Desai, S., Kohli, V., Hunter, W., Uhl, J. D., Rost, M. S. and Sumanas, S. (2012). Hedgehog signaling is required for differentiation of endocardial progenitors in zebrafish. *Dev. Biol.* **361**, 377-391.

Zhang, R., Han, P., Yang, H., Ouyang, K., Lee, D., Lin, Y.-F., Ocorr, K., Kang, G., Chen, J., Stainier, D. Y. et al. (2013). In vivo cardiac reprogramming contributes to zebrafish heart regeneration. *Nature* **498**, 497-501.

Zhao, Q., Beck, A. J., Vitale, J. M., Schneider, J. S., Gao, S., Chang, C., Elson, G., Leibovich, S. J., Park, J. Y., Tian, B. et al. (2011). Developmental ablation of Id1 and Id3 genes in the vasculature leads to postnatal cardiac phenotypes. *Dev. Biol.* **349**, 53-64.

Zhao, L., Borikova, A. L., Ben-Yair, R., Guner-Ataman, B., MacRae, C. A., Lee, R. T., Burns, C. G. and Burns, C. E. (2014). Notch signaling regulates cardiomyocyte proliferation during zebrafish heart regeneration. *Proc. Natl. Acad. Sci. USA* **111**, 1403-1408.

Supplementary Information

Supplementary Material and Methods

Zebrafish transgenic lines

We used the following fish lines: WT AB strain, *ET(krt4:EGFP)*$^{sqet33\text{-}mi60A}$ (*ET33-mi60A*), *ET(krt4:EGFP)*$^{sqet33\text{-}1A}$ (*ET33-1A*) (Poon et al., 2010), *Tg(hsp70l:Gal4)*^{kca4}*;Tg(UAS:myc-Notch1a-intra)*^{kca3}, [abbreviated here as *Tg(UAS:NICD)*] (Scheer et al., 2001), and *Tg(fli1a:GFP)y1* (Lawson and Weinstein, 2002), *Tg(myl7:mRFP*) (Rohr et al., 2008).

Treatments

Heat shocks to *Tg(UAS:NICD)* fish were applied automatically as described (Munch et al., 2013). Regimes for heat shock applications of each experiments are indicated in the corresponding figure. For short-term experiments (1-3 dpci, 1-7 dpci) we applied 40 min heat shocks and for long-term experiments (1-33 dpci, 1-90 dpci) a 1-h heat shock. Control animals for these experiments were *Tg(hsp70l:Gal4)*^{kca4} or *Tg(UAS:myc-Notch1a-intra)*^{kca3} fish. BrdU (30 µl, 2.5 mg/ml in PBS) was administered intraperitoneally at 2 dpci (for endocardial proliferation analysis) or at 5 and 6 dpci (for myocardial proliferation analysis).

Histology

All antibodies used in our studies have been tested elsewhere. We used the following antibodies: GFP (1:100, Living Colors, rabbit, C#632592, and mouse, C#632381) (Gonzalez-Rosa et al., 2011), GFP (1:500, Aves, chicken, GFP-1010) (Zhang et al., 2013), BrdU (1:30, BD, ab6326) (Munch et al., 2013), Delta-4 (1:100, Santa Cruz Biotechnology, rabbit, sc-28915) (D'Amato et al., 2016), collagen type I (1: 100, DSHB, SP1.D8, mouse, C#SP1.D8,RRID:AB_528438) (Gonzalez-Rosa et al., 2011), myosin heavy chain (1:100,

MF20, DSHB, mouse, C#MF20RRID:AB_2147781) (Gonzalez-Rosa et al., 2011), ERG (1:200, Abcam, rabbit, ab110639) (Bednarek et al., 2015) and Mef-2 (1:100, Santa Cruz Biotechnology, rabbit, sc-313) (Bednarek et al., 2015) Phalloidin Congutated to FITC (1:50, Sigma-Aldrich, P5282). For IHC against Delta-4 and collagen type-1 the signal was amplified with secondary antibodies coupled to horseradish peroxidase (1:100, Dako Cytomation, P0447-8) and tyramides coupled to Cy3 (1:100, TSA, Perkin Elmer, NEL744001KT) (Luxan et al., 2013). ISH was performed as described (Kanzler et al., 1998) using the following probes: *atf3* (Chen et al., 2012), *lfng* (Prince et al., 2001), *hand2* (Yelon et al., 2000), *nkx2.5* (Chen and Fishman, 1996), *notch1b*, *notch2*, *notch3* (Westin and Lardelli, 1997), *cdh5* (Larson et al., 2004), *mmp9*, *nfatc1a, klf2a* (Vermot et al., 2009) and *l-plastin* (Yoshinari et al., 2009). Primer sequences for new probes can be found in Table S7. For fluorescence ISH (FISH), we followed the same protocol (Kanzler et al., 1998), however we used a peroxidase-coupled antibody for DIG-labelled mRNA-probe detection. We developed the signal using tyramides coupled to Cy3 (TSA, Perkin Elmer, 1:200) and subsequently performed IHC after several washed with PBS. AFOG staining was as described previously (Kikuchi et al., 2011).

Imaging

Whole mount images were obtained with an Olympus DP71 camera fitted to a Leica stereomicroscope. For whole mount 3D imaging, hearts were fixed in 2% PFA overnight. Following 3 washes in PBS, hearts were incubated in CUBIC reagent 1 (Susaki et al., 2014) at 37ºC overnight. Using a Leica TCS SP-5 confocal microscope, we scanned 900 µm of whole hearts (Figs. 1G-J, 4D, S1E) taking z-stacks every 7 µm with a 10x objective or 200 µm with z-stacks every 3 µm for imaging with the 20x objective (Figs. 2A,2C,3C,4F,S5E). Images of ISH and immune-stained heart sections were taken with a DP71 camera fitted to an Olympus BX51 microscope. For confocal images of immune-stained heart sections, we used a Leica TCS SP-5 or Nikon A1-R confocal microscope.

Gene expression analysis

Power SYBR Green Master Mix (Applied Biosystems) was used for qPCR with the ABI PRISM 7900HT FAST Real-Time PCR System. Gene expression levels were calculated relative to *elf1a* or *rpsm* and then compared with gene activation in samples taken from non-injured hearts (wild-type gene expression analysis) from DMSO-treated samples (for RO treatment experiments) or from *Tg(hsp70l:Gal4)*^{kca4} or *Tg(UAS:myc-Notch1a-intra)*^{kca3} heart samples (for Notch overactivation experiments). RNA-extraction

and cDNA synthesis of PAVEC were conducted accordingly. Quantitative RT-PCR was performed as described before. Data shown represent the mean ± s.d. of three separate experiments. Gene expression levels were calculated relative to *GADPH* and then compared with gene activation DMSO-treated samples.

Quantification and statistical analysis

Experiments were performed on 3- 9 biological replicates to ensure adequate statistical power to detect specific effects. Detailed information on the sample size of each experiment can be found in Table S1 and Table S2.

For 3D volume rendering and volume quantification, we used IMARIS x64 software, with manual selection of the injured region (myl7:mRFP). A mask of this region was used to select the GFP^+ endocardium within the injury site, and the volumes of both were calculated and compared (See Fig. 1K). Graphs represent values of individual hearts and means ± standard deviation (s.d.). Statistical significance was calculated with One-way ANOVA combined with the Newman-Keuls method for multiple comparisons. Filopodia like protrusions of the injury-induced endocardium (Figs. 2C, D, 3H,I) were quantified on randomly selected regions (513 µm x 513 µm x 10 µm) within the whole scanned region, 3-5 per heart. The graphs represent mean values of individual hearts and means ± s.d. Statistical significance was calculated with Student's t-test.

The amount of fibrotic tissue on AFOG-stained heart sections, labelling fibrin and collagen deposition, was measured as follows. ImageJ/ Fiji (http://imagej.net/ImageJ) was used to determine the size of the injured area relative to the size of the ventricle on at least four sections taken at four different levels throughout the heart, so that the size of the injury site at different levels of the heart was represented. The mean value was then calculated. This allows estimation of the 3D volume of the injury site. For quantifications of immunofluorescent or ISH stainings, heart sections were selected randomly. It was assured that the injury site throughout the heart was represented by staining one slide containing sections of different levels of the heart (see Histology section). BrdU incorporation was estimated as the ratio of BrdU-labelled $Mef2^+$ cardiomyocytes to the total number of $Mef2^+$ cardiomyocytes flanking the injured area. We analysed 7-8 hearts and 4-8 sections per heart. Accordingly, endocardial cell proliferation and the percentage of endocardial cells expressing *serpine1* were estimated using 4- 6 hearts per time point and condition and analysing 4- 6 sections per heart. For macrophage quantification, only *l-plastin*- or

mpeg1-expressing cells within the injury site but not in the outer epicardial region were considered. To estimate cardiomyocyte density, the number of $Mef2^{+}$ cardiomyocytes adjacent to the injury site was divided by their area. Graphs represent values of individual hearts and means ± standard deviation. We expected normal distributions of the parameters analysed in our experiments, with similar variances in the experimental groups. Statistical significance was calculated with the two-tailed Student's t-test or with One-way ANOVA combined with the Newman-Keuls method for multiple comparisons.

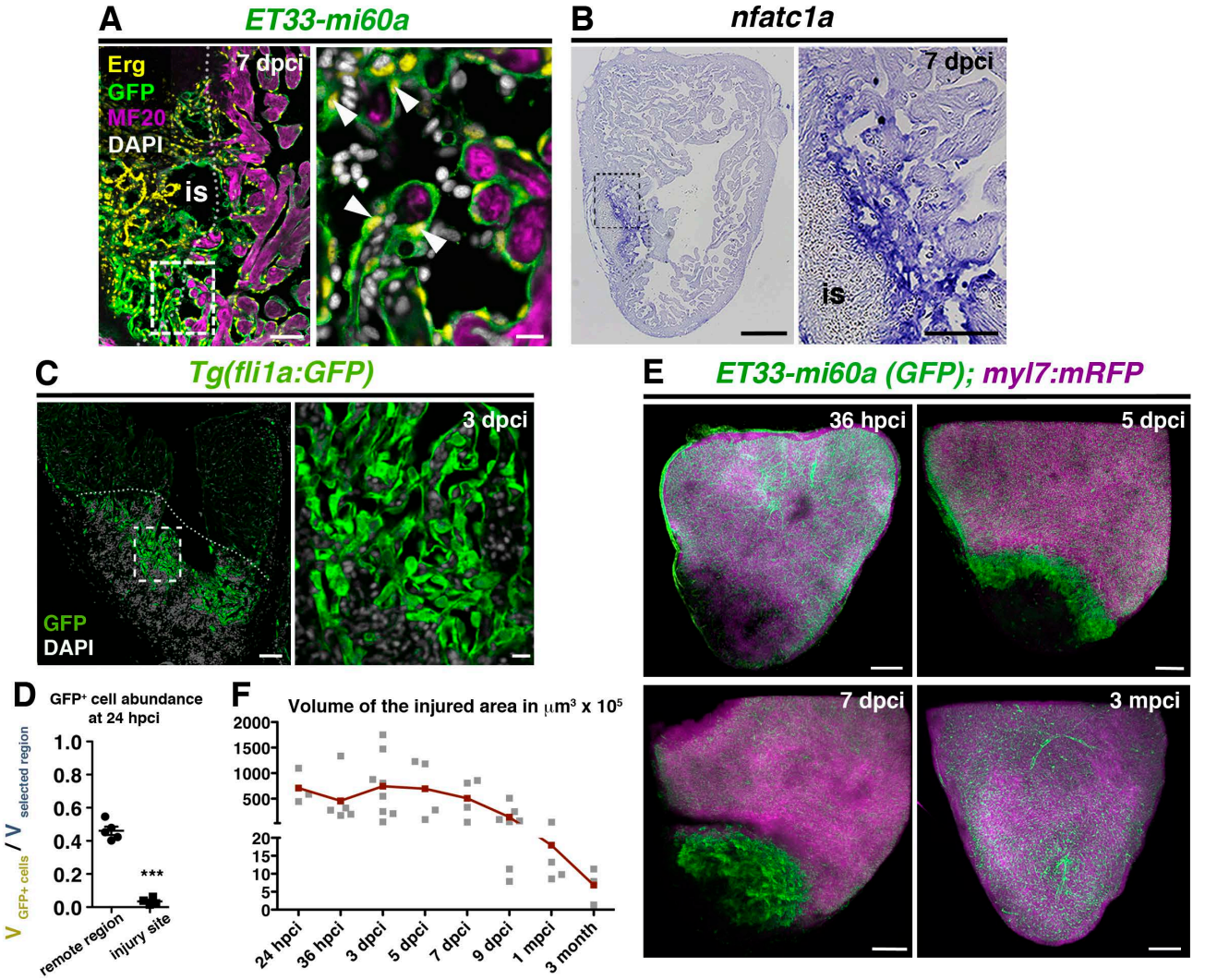

Fig. S1: Activated endocardium in the injury site

(A) IHC against ERG, GFP and MF20 on sections of *ET33-mi60a* transgenic hearts (7 dpci), showing GFP^+ endocardial/endothelial cells within and lining the injury site (is) (white arrowheads). The boxed area is magnified in the right-hand panel. (B) ISH against *nfatc1a* at 7 dpci, showing strong expression within the injury site (is). (C) IHC against GFP on sections of *Tg(fli1a:GFP)* transgenic hearts (3 dpci) showing endocardial cells at the injury site. The boxed area is magnified in the right-hand panel. (D) Scatter plot showing the relative volume occupied by GFP^+ cells in a selected region of the remote region and the injury site at 24 hpci. Values of endocardial volume at the injury site are also represented in Figure 1L (black line = mean ± s.d, t-test, $***P<0.005$). (E) Volume rendering of injured ventricles of *ET33mi-60A; myl7mRFP* hearts, with endocardium labelled green and myocardium magenta, at indicated time points. Volume rendering movies are available in the expanded view section. (F) Scatter plot showing the evolution of injury-site volume after cryoinjury in *ET33-mi60a; myl7:mRFP* transgenic hearts, quantified with IMARIS. (G-I) IHC against GFP and Pcna on sections of *ET33-mi60a* transgenic hearts (no ci, 3 dpci, 5dpci), showing almost any Pcna-expressing endocardial cell in the non-injured heart but high abundance of proliferating cells within the injury site (is) at 3 and 5 dpci (white arrowheads). The boxed area is magnified in the right hand panel. The dotted lines demarcate the injured tissue. Scale bars: 50 μm in A; 200 μm in B, E; 100 μm in C, G, H, I; 5 μm in magnified views in A, 100 μm in B, 20 μm in C,G, I.

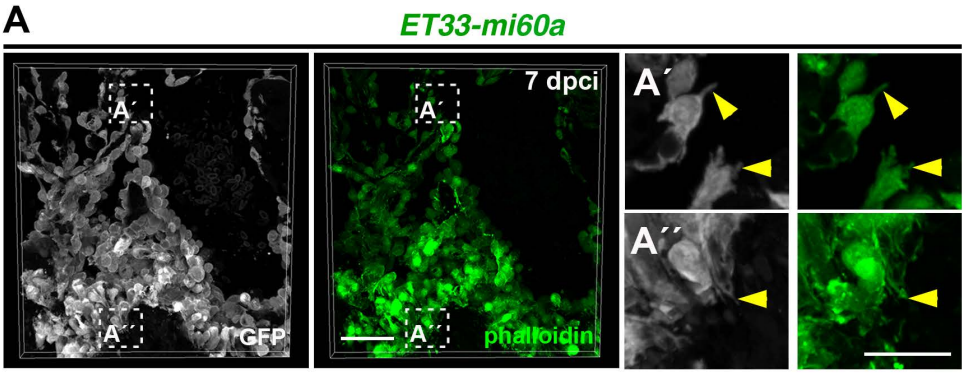

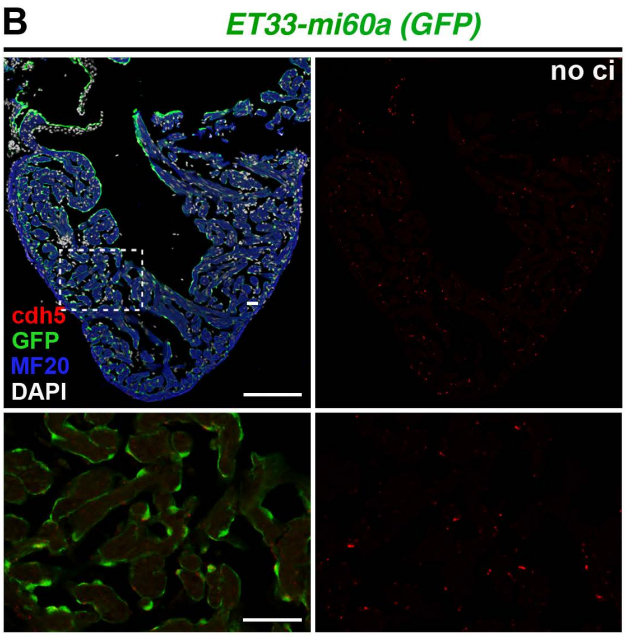

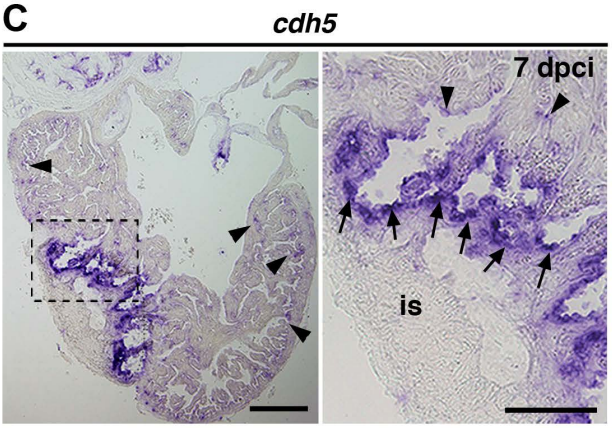

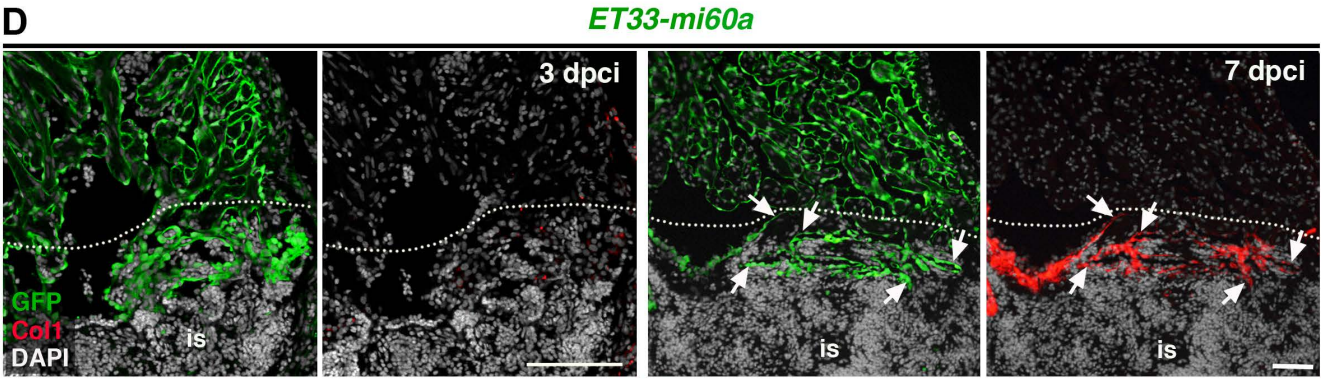

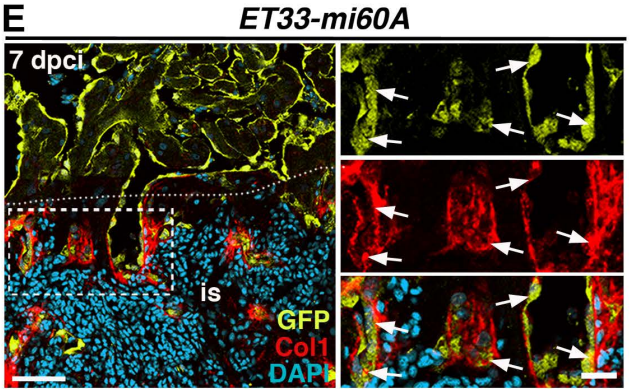

Fig. S2 The injury endocardium exhibits filopodia-like protrusions and high levels of cdh5

(A) Vibratome section of *ET33-mi60A* heart, immune-stained for GFP and with phalloidin (7 dpci). Filopodia-like protrusions of wound endocardial cells show phalloidin staining (A´, A´´, arrowheads) (B) *cdh5* FISH combined with IF showing low levels of *cdh5* levels (red) in GFP^+ endocardial cells all over the ventricle. (C) ISH against *cdh5* at 7 dpci, showing strong expression within the injury site (is, arrow) and weak expression in the remote region (arrowheads). Boxed areas are magnified below or on the right. (D, E) IHC against GFP and Col1 on sections of *ET33-mi60a* transgenic hearts, showing low Col1 signal at 3 dpci (B) and similar distribution of endocardial cells and col1 at the inner injury border (dotted line) at 7dpci (C, white arrowheads). Scale bars: 50 μm in A, E; 200 μm in B, C; 100 μm in D, 25 μm in magnified views in A, E, 50 μm in B, C.

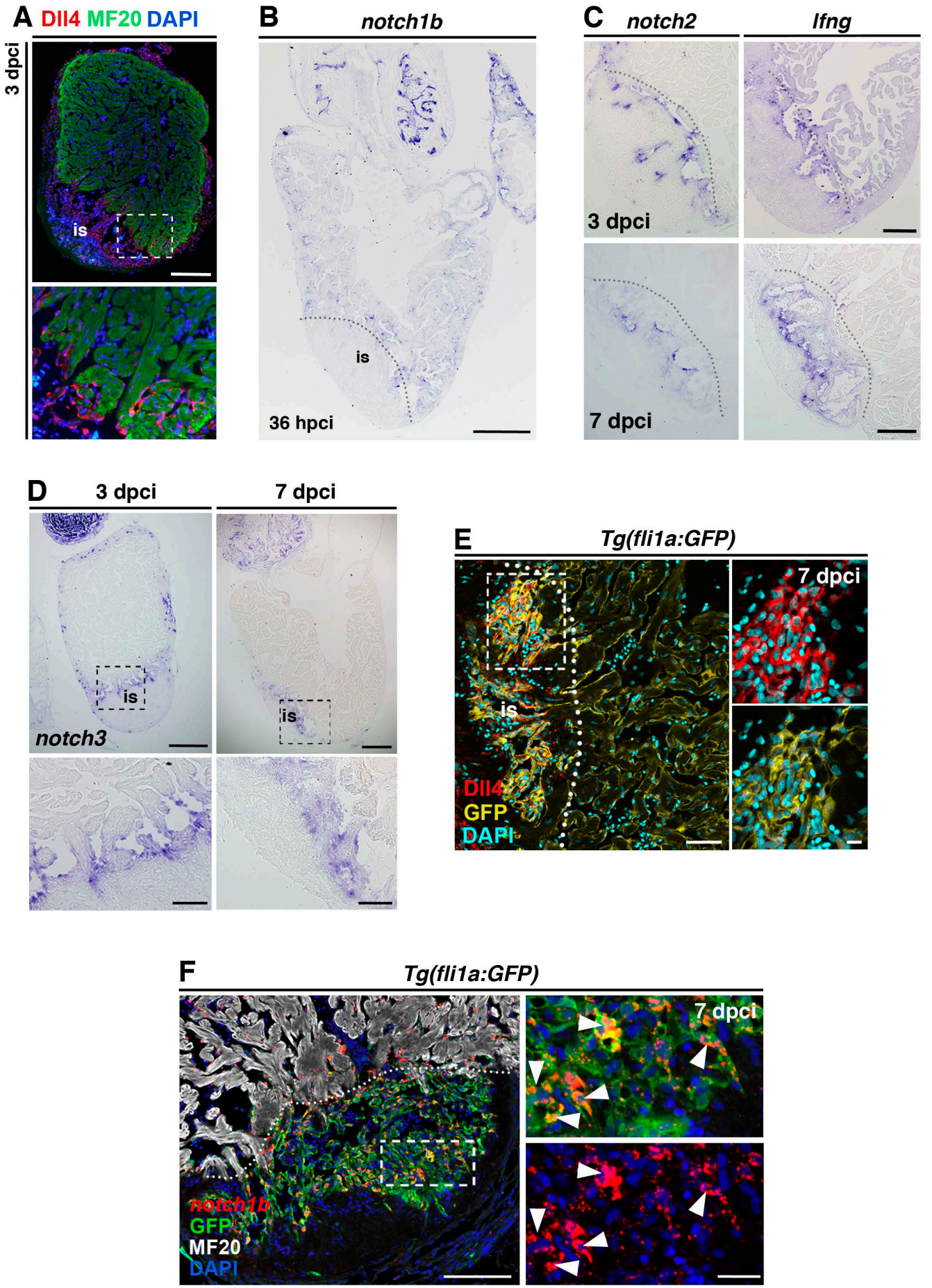

Fig. S3: Genes encoding Notch signalling elements are expressed in endocardial cells upon cryoinjury

(A) IHC of Dll4 and MF20, showing expression within the injury site (is) and surrounding adjacent cardiomyocytes. The boxed area is magnified in the panel below. (B) ISH for *notch1b*, showing low *notch1b* expression in the injury site and the remote region at 36 hpci. The dotted line demarcates the injury site (is). (C, D) ISH of *lfng*, *notch2* and *notch3* in regenerating hearts, showing expression adjacent to and within the injury site (is; 3 dpci, 7 dpci). Boxed areas are shown at higher magnification in the lower row. (E) IHC against Dll4 and GFP on sections of *Tg(fli1a:GFP)* transgenic hearts (7 dpci), showing endocardial expression of Dll4 (white arrowheads). The dotted line demarcates the injury site (is). (F) FISH against *notch1b* combined with IHC against GFP and MF20 on sections of *Tg(fli1a:GFP)* transgenic hearts (7 dpci) showing *notch1b* transcripts in endocardial cells (white arrowheads). The boxed area is magnified in the right-hand panels. The dotted line demarcates the injury site (is). (Scale bars: 200 μm in A, B; 100 μm in C, D, E, F; 50 μm in magnified views in A, D; 20 μm in E, F.

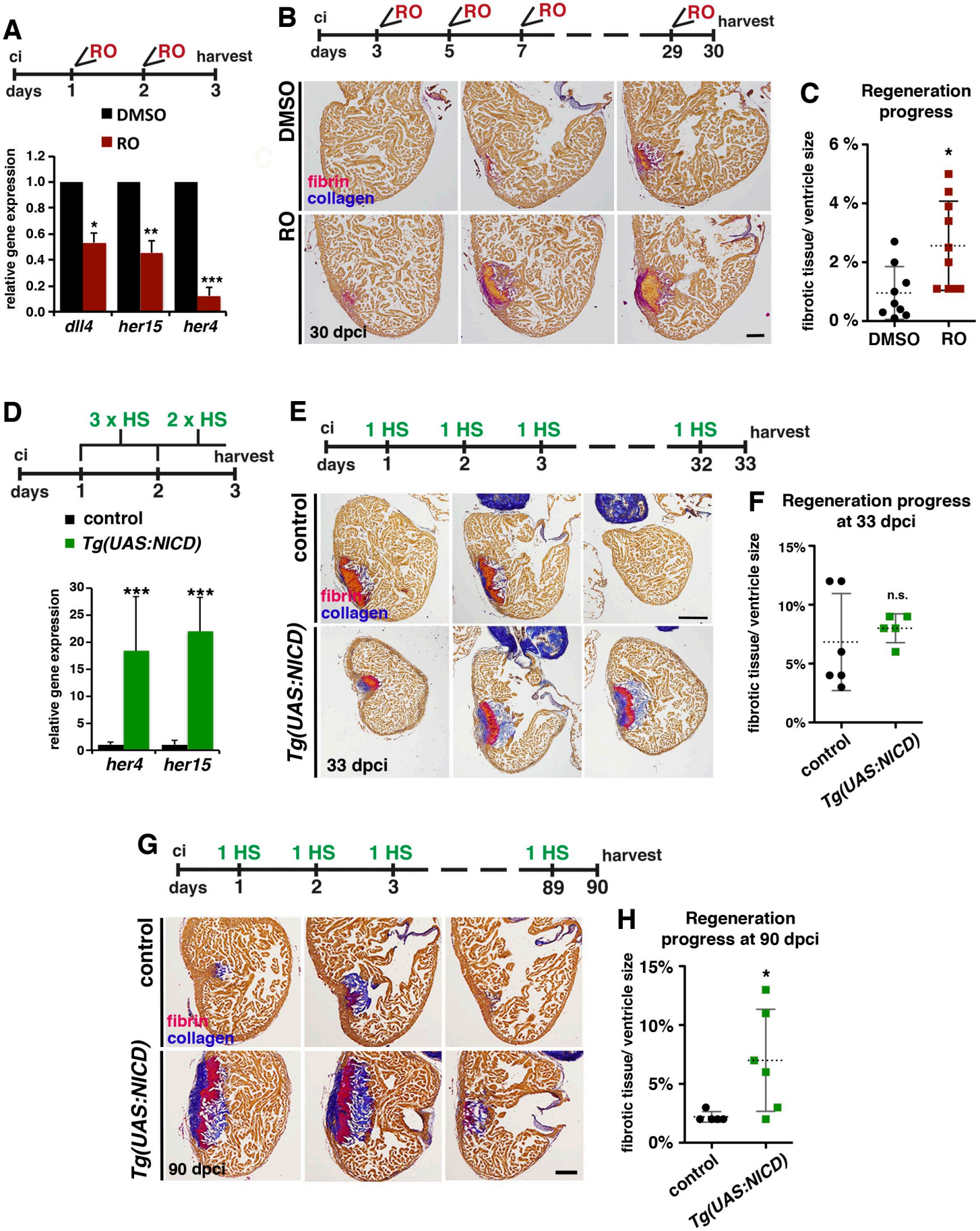

Figure S4_Münch et al.

Fig. S4: Notch signalling modulation impairs heart regeneration

(A) Relative gene expression (qPCR) of the Notch target genes *dll4*, *her15*, and *her4*, showing reduced expression after RO treatment (indicated on top). * $P<0.05$; ** $P<0.01$; *** $P<0.005$. (B) Representative AFOG-stained sections from three levels of the hearts of fish treated with DMSO or RO for 30 dpci (treatment regime is indicated on top). Cardiac muscle: brown; fibrin: pink/ orange; collagen: blue. (C) Scatter plot showing the amount of fibrotic tissue relative to ventricle size in hearts from fish treated with DMSO or RO (discontinuous line = mean ± s.d, t-test * $P<0.05$) (D) qPCR showing higher expression of *her4* and *her15* in injured hearts of transgenic *Tg(UAS:NICD)* fish compared than in the control at 3 dpci. (heat shock regime is indicated on top (mean ± s.d, t-test, *** $P< 0.005$). (E) AFOG–stained sections taken at 3 anatomical levels of WT and *Tg(UAS:NICD)* hearts at 33 dpci, showing similar regenerative capacity (heat shock regime is indicated on top). (F) Quantification of the progress of regeneration at 33 dpci (discontinuous line = mean± s.d, t-test, not significant). (G) AFOG-stained sections taken at 3 anatomical levels of WT and *Tg(UAS:NICD)* hearts at 90 dpci, showing failed regeneration (heat shock regime is indicated on top). (H) Quantification of the progress of regeneration at 90 dpci (discontinuous line = mean, t-test * $P<0.05$). Scale bars: 100 μm.

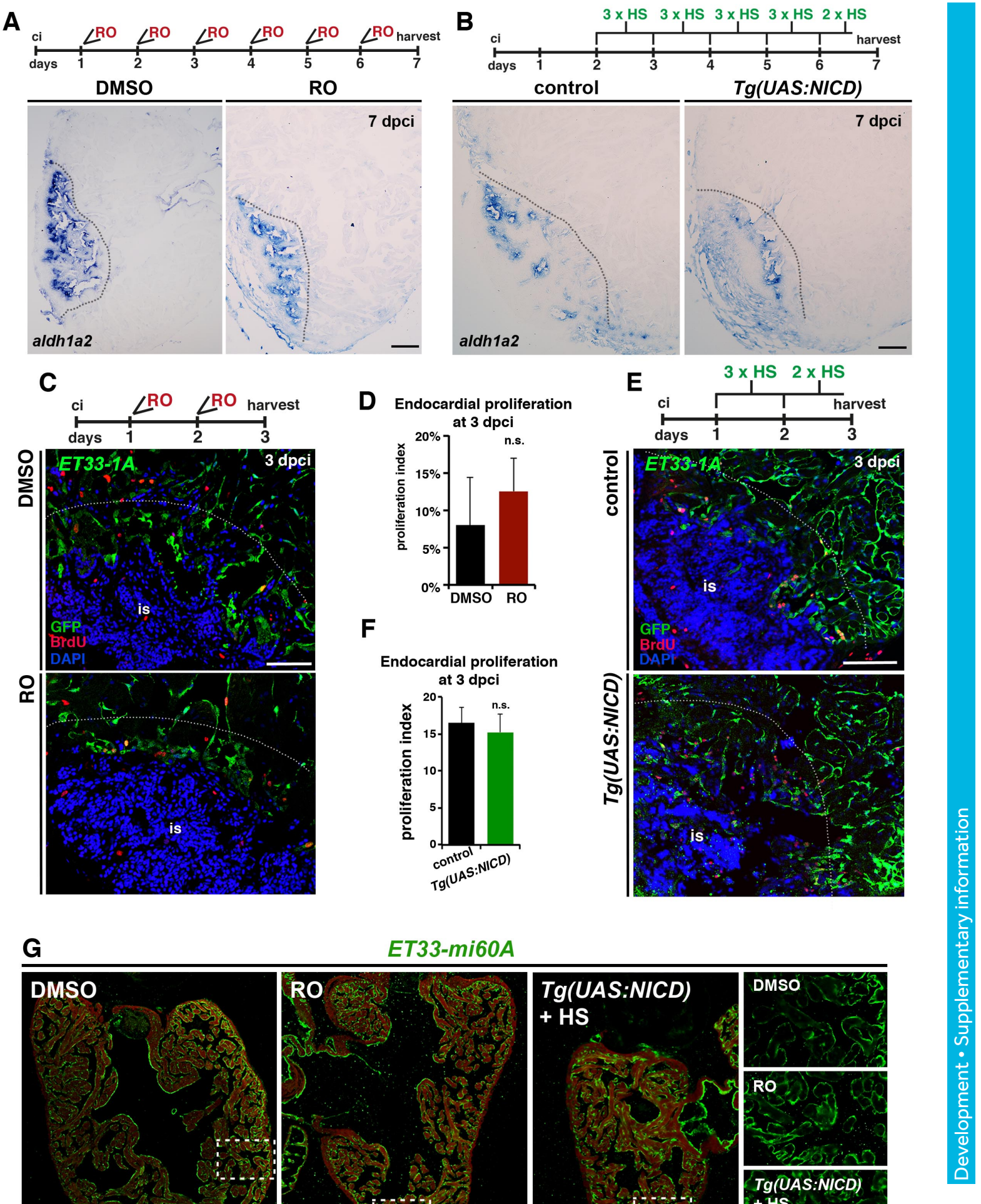

Fig. S5: Notch signalling modulation does not affect *aldh1a2* expression or proliferation

(A,B) ISH for *aldh1a2* on sections of hearts treated with DMSO or RO or from heat-shocked *Tg(UAS:NICD)* and control fish, showing no differences of expression. RO-treatment and heat shock regimes are indicated on top. (C) IHC against BrdU and GFP on heart sections of *ET33-1a* transgenic fish (3 dpci), showing BrdU incorporation by GFP^+ endocardial cells adjacent to the injury site (is). (D) Quantification of $BrdU^+$/ GFP^+ cell ratio in hearts of fish treated with DMSO or RO, indicating no difference in endocardial cell proliferation (mean± s.d, t-test, not significant). (E) IHC against BrdU and GFP on heart sections of *ET33-1a* transgenic fish alone or crossed with *Tg(UAS:NICD)* at 3 dpci, showing BrdU incorporation by GFP^+ endocardial cells adjacent to the injury site (is). (F) $BrdU^+$/ GFP^+ cell ratio in hearts of *ET33-1a* and *Tg(UAS:NICD); ET33-1a* transgenic fish, indicating no difference in endocardial cell proliferation (mean± s.d, t-test, not significant). (G) IHC for GFP and mf20 on sections of hearts treated with DMSO or RO or from heat-shocked *Tg(UAS:NICD)*, showing no differences of expression. Boxed areas are magnified on the right. Hearts were treated for 3 days with RO, DMSO or heat shocks. Scale bars: (A) 100 μm in all panels.

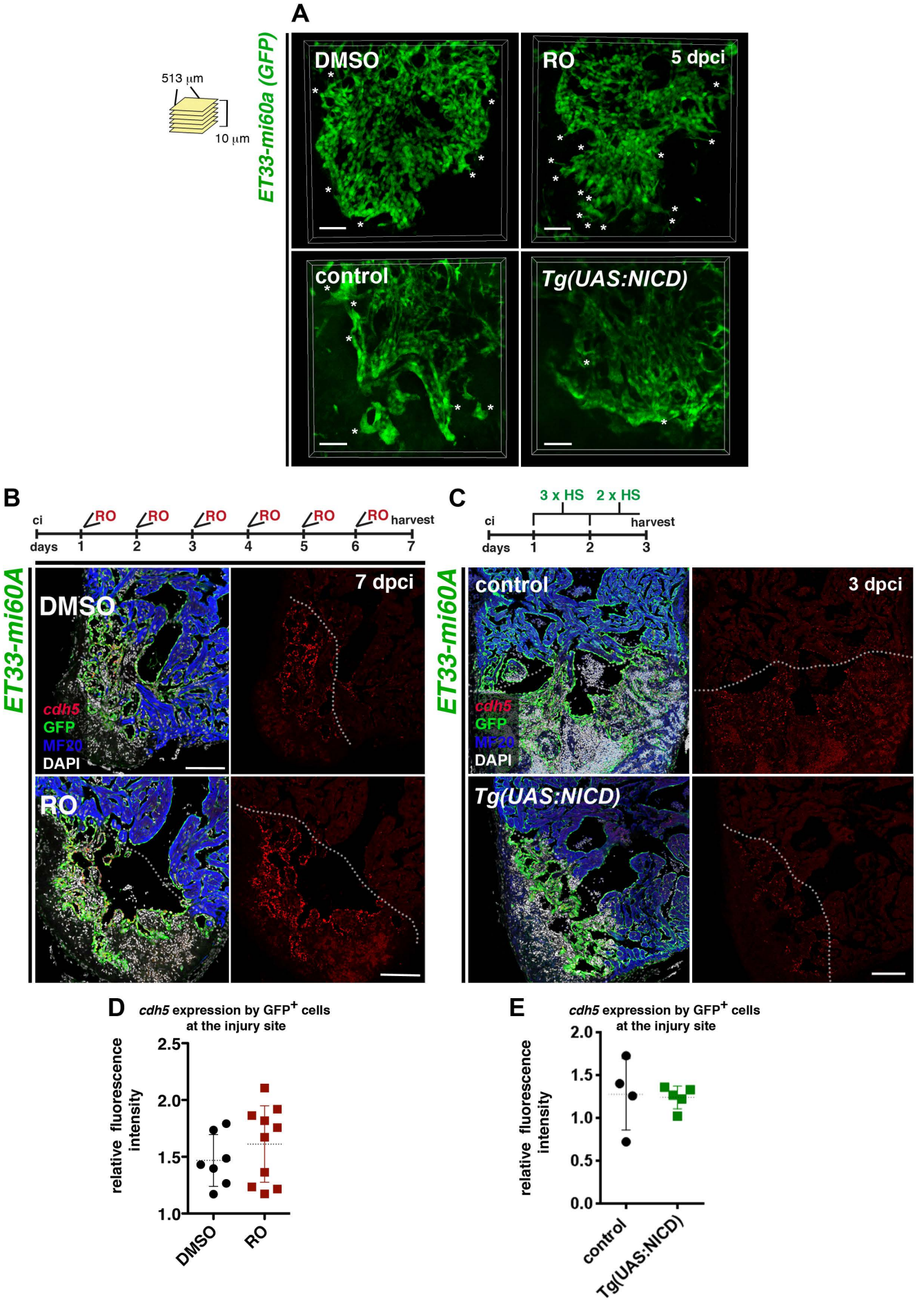

Fig. S6 Notch signalling modulation does not interfere with endocardial *cdh5*-expression

(A) Volume rendering of part of the injured region (513 µm x 513 µm x 10 µm) from *ET33mi-60A; myl7mRFP* hearts after treatment with RO or DMSO and from *ET33mi-60A; myl7mRFP, Tg(UAS:NICD)* and control hearts. Comparable 3D-images were used for quantification of filopodia- like protrusions. The graph of quantified filopodia is shown in Figure 3I. (B, C) FISH against *cdh5* combined with IHC against GFP and mf20 on sections of *ET33-mi60a* transgenic hearts after treatment with DMOS or RO (7dpci) and of *ET33mi-60A;Tg(UAS:NICD)* and control hearts (3dpci). The treatment regime is indicated on top. GFP^{+} endocardial/endothelial cells at the injury site present similar levels of *cdh5* expression in injured hearts after treatment with RO or DMSO and in *ET33mi-60A;Tg(UAS:NICD)* or control hearts. (D, E) Scatter plot showing relative red fluorescence intensity, comparing values of the endocardium of the remote region to the injury endocardium (see Figure 2D), in injured hearts (dotted line = mean± s.d, t-test, not significant). Scale bars: 50 µm in A, 100 µm in B, C.

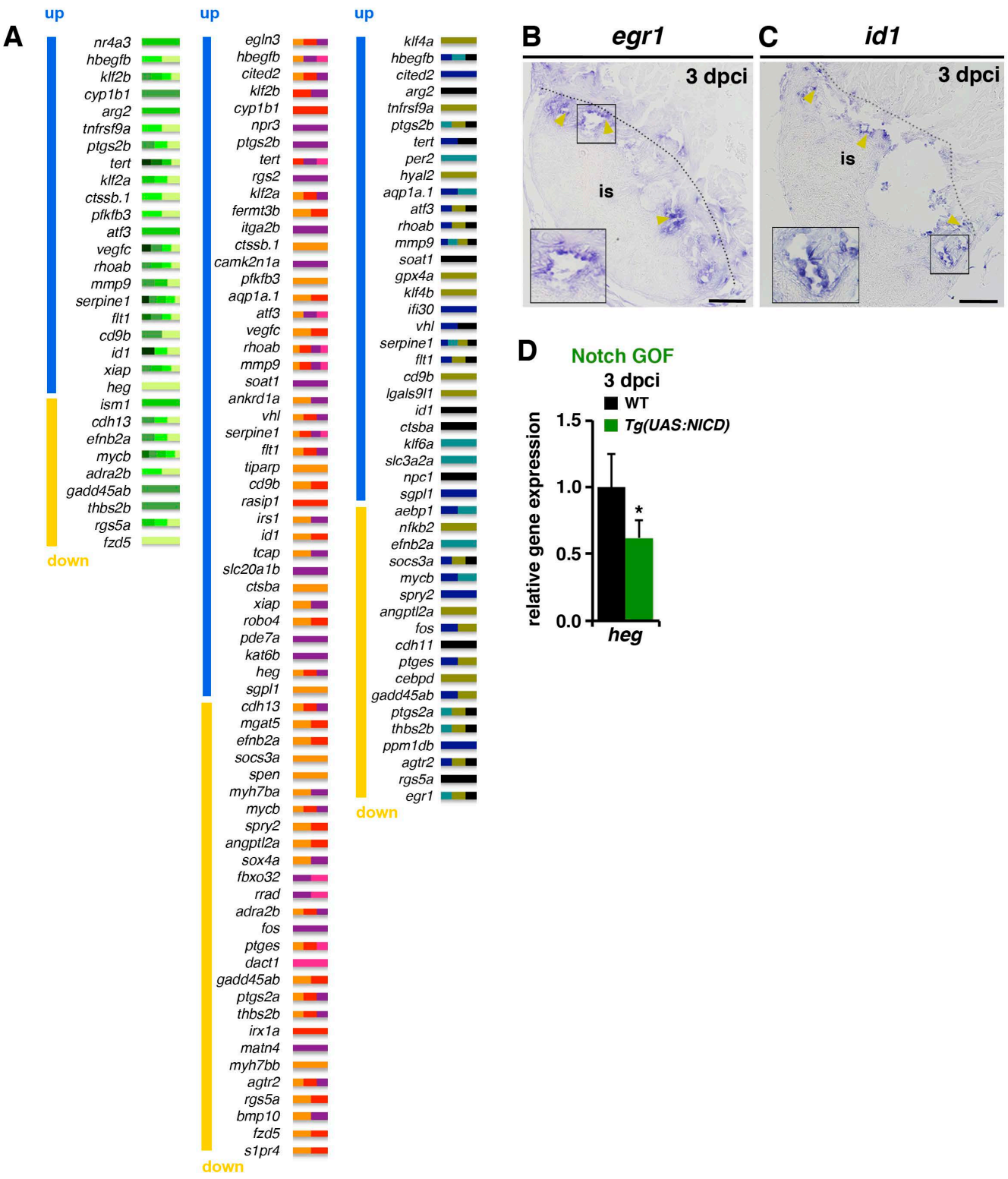

Fig. S7: Notch signalling affects endocardial/endothelial gene expression

(A) Genes assigned to the three categories in (Figure 4I). Genes are ordered according to their level of differential expression (up-regulated upon RO-treatment, blue; down-regulated, yellow). The colour of small bars indicates the assigned Ingenuity categories (presented in the chart in Figure 4C). (B, C) ISH,

showing *egr1*- and *id1*- expression at the inner injury border (yellow arrowheads). The boxed area is magnified in inserts. (D) qPCR analysis showing lower *heg* mRNA levels in *Tg(UAS:NICD)* transgenic injured ventricles than in control. (mean± s.d., t-test, **P*<0.05). Dotted lines delineate the injury site (is). Scale bars: 100 μm.

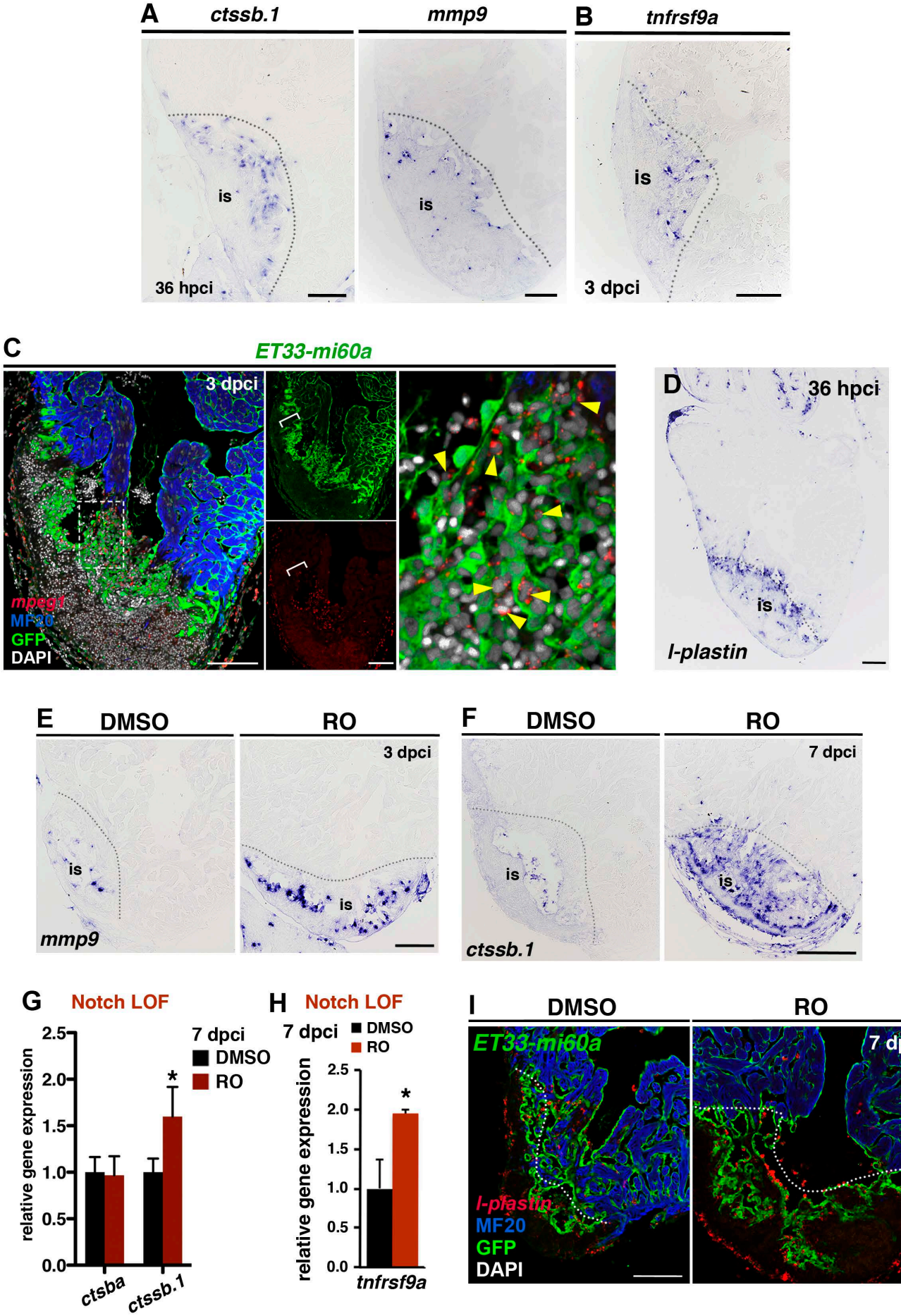

Fig. S8: Notch inhibition affects ECM remodelling gene expression and inflammatory processes

(A) ISH for *ctssb.1* and *mmp9*, revealing high expression at the inner injury border at 36 hpci. (B) ISH against *tnfrsf9a* on sections from an injured ventricle at 3 dpci, showing gene expression in cells with endocardial morphology within the injury site. (C) *mpeg1*- FISH combined with IHC, showing *mpeg*$^{+}$ cells (yellow arrowheads) in contact with GFP^{+} cells. *mpeg1*$^{+}$ cell accumulations at the injury site (is) locally coincides with high endocardial cell abundance (brackets). (D) ISH on consecutive sections for *l-plastin* showing high *l-plastin* expression in the injury site at 36 hpci. (E) ISH against *mmp9* (3 dpci), showing high numbers of positive cells within the injury site (is) of RO-treated hearts. (F) ISH against *ctssb.1* (7 dpci), showing high numbers of positive cells within the injury site (is) of RO-treated hearts. (G) qPCR analysis showing increased *ctssb.1* mRNA levels in injured ventricles at 7 dpci after RO-treatment. (mean± s.d., t-test, **P*<0.05. (H) qPCR analysis of *tnfrsf9a* expression in ventricles at 7 dpci after treatment with RO or DMSO mean± s.d., t-test, **P*<0.05). (I) FISH against *l-plastin* combined with IHC against GFP and MF20 on sections of *ET33-mi60a* transgenic hearts (7 dpci) after RO- or DMSO-treatment. RO-treatment results in an increased abundance of l-plastin^{+} macrophages associated to the endocardium. Dotted lines delineate the injury site (is). Scale bars: 100 µm.

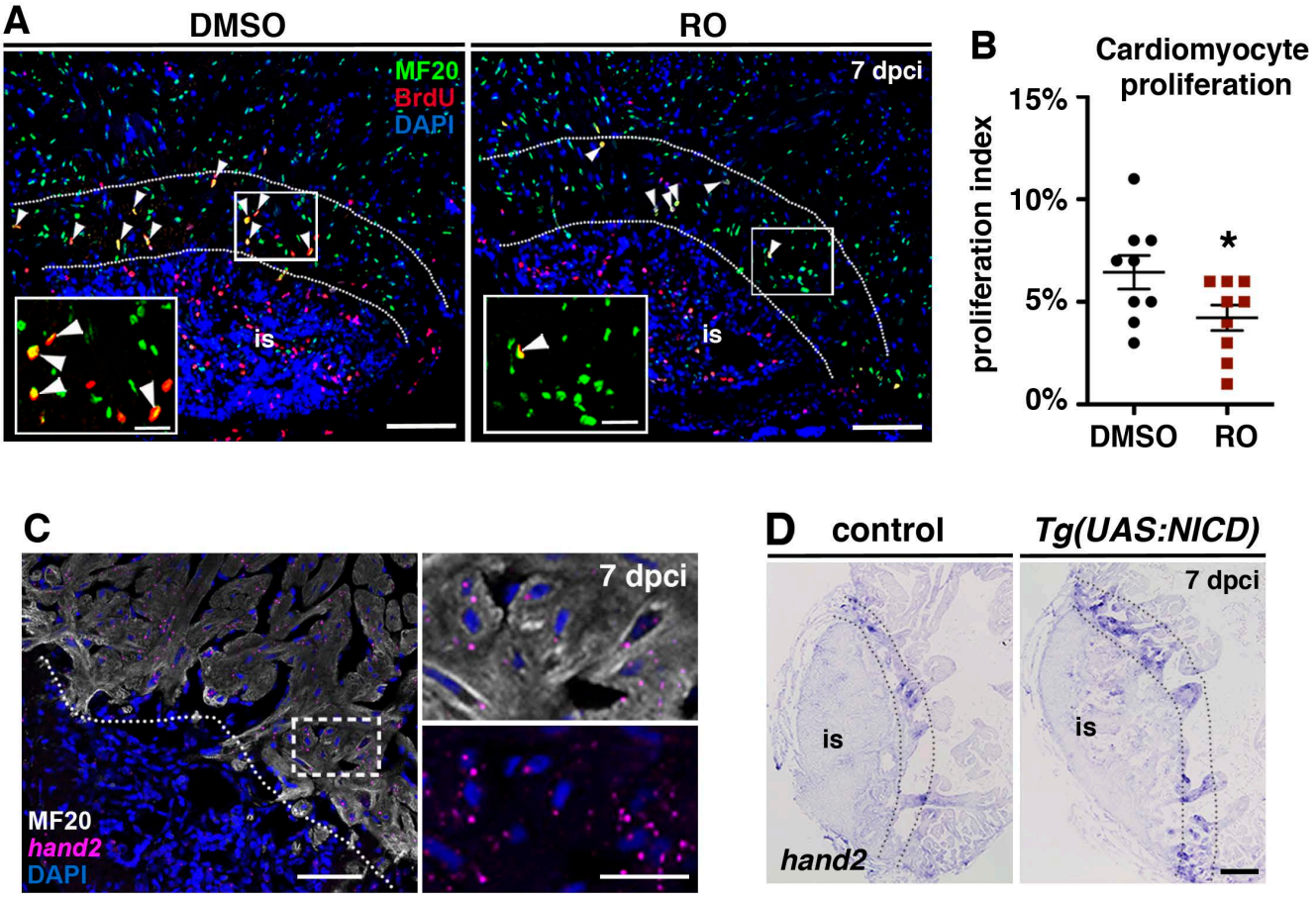

Fig. S9: Notch inhibition decreases cardiomyocyte proliferation

(A) IHC against BrdU and Mef2 on heart sections (7 dpci), showing lower BrdU incorporation in $Mef2^+$ cells (white arrowheads) adjacent to the injury (between the dashed lines) after treatment with RO than after treatment with DMSO. (B) Scatter plot showing quantification of $BrdU^+$ $Mef2^+$ cells in DMSO- and RO-treated hearts (discontinuous line = mean ± s.d., t-test, $*P<0.05$). (C) FISH against *hand2* combined with IHC for mf20 showing, *hand2*-expression in cardiomyocytes. (D) ISH against *hand2* at 7 dpci, showing higher numbers of injury-adjacent cardiomyocytes expressing these genes (between the dotted lines) in *Tg(UAS:NICD)* hearts than in control hearts. Dotted lines delineate the injury site (is). Scale bars: 100 µm; 25 µm in amplified views.

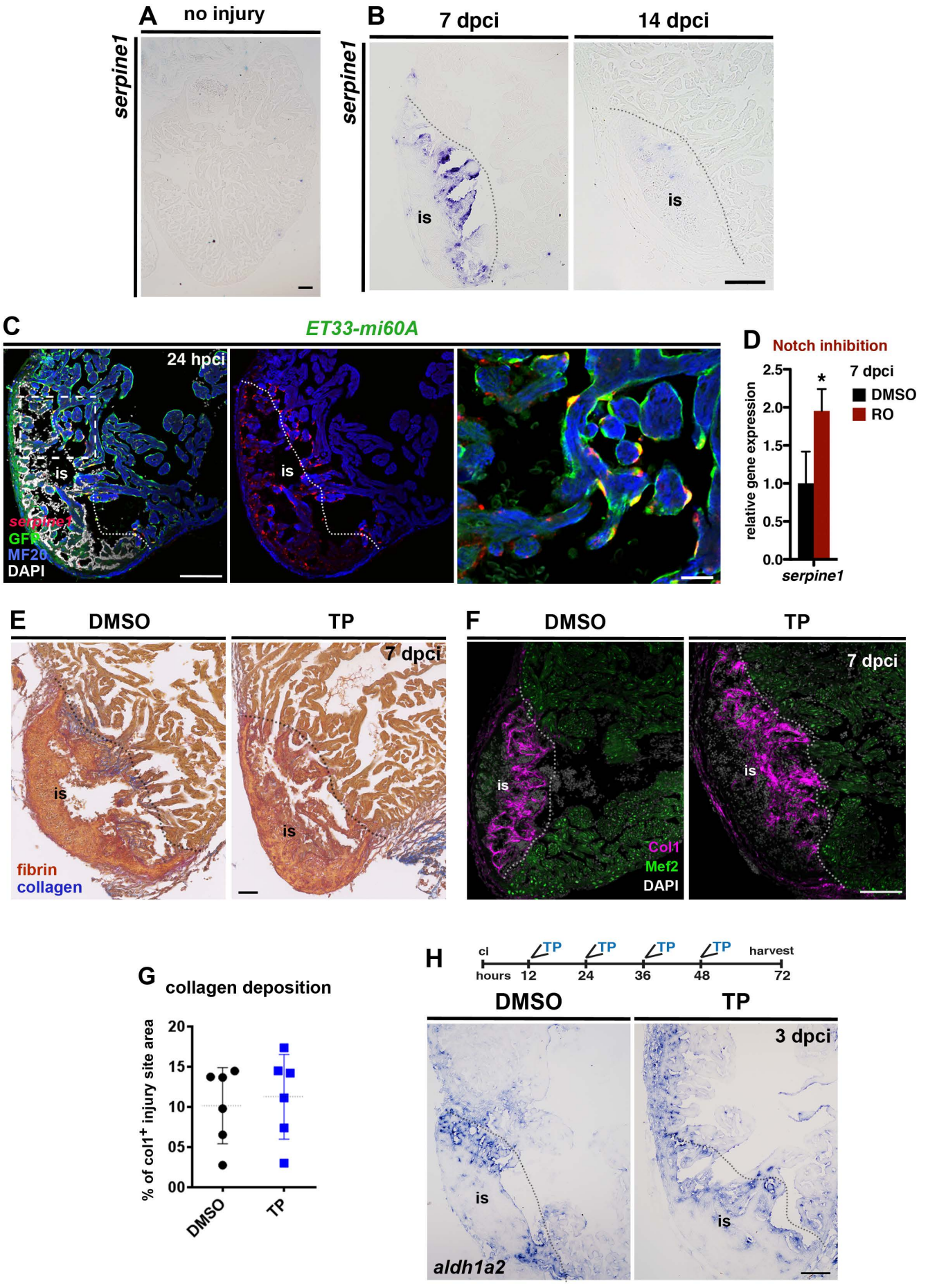

Fig. S10 Serpine1 is upregulated in the injury endocardium and its inhibition does not interfere with blood clot or collagen deposition.

(A, B) ISH against *serpine1*, showing no expression in the uninjured heart, moderate levels at 7 dpci but almost no expression at 14 dpci. (C) FISH against *serpine1* combined with IHC against GFP and MF20 on sections of *ET33-mi60a* transgenic hearts at 24 hpci. Serpine1 is strongly expressed in GFP^+ endocardial cells adjacent and within the injury site but not in remote regions at 24 hpci. The boxed area is magnified on the right hand panel. (D) qPCR analysis showing higher *serpine1* mRNA levels in injured ventricles at 7 dpci in RO-treated fish than in DMSO-treated fish (mean± s.d., t-test, $*P<0.05$). (E) AFOG stained TP- or DMSO treated hearts indicating similar fibrin deposition at the injury site (is) in both groups at 7dpci. (F) IHC for collagen 1 (Col1) and Mef2 showing similar amount of collagen at the injury site upon TP or DMSO-treatment. (G) Scatter plot showing the area covered by collagen relative to the injury site area in hearts treated with TP or DMSO. (dotted line = mean± s.d, t-test, not significant). (H) ISH in hearts treated with TP or DMSO (regime is indicated on top) showing similar expression of *aldh1a2* in the injury endocardium. Dotted lines delineate the injury site (is). Scale bar: 100 μm; 20 μm in the amplified view in C.

Supplemental Tables

Table S1: Sample numbers Figure 1-7 (Excell file attached)

Click here to Download Table S1

Table S2: Sample numbers Figure S1- S10 (Excell file attached)

Click here to Download Table S2

Table S3: Newman-Keuls Multiple Comparison Test for relative GFP^+ cell volume at indicated time points (Figure 1L)

Sample comparison	Significant? P < 0.05?	Summary
24 hpci vs 3 mpci	Yes	***
24 hpci vs 1 mpci	Yes	***
24 hpci vs 7 dpci	Yes	***
24 hpci vs 9 dpci	Yes	***
24 hpci vs 5 dpci	Yes	***
24 hpci vs 3 dpci	No	**ns**
24 hpci vs 36 hpci	No	**ns**
36 hpci vs 3 mpci	Yes	***
36 hpci vs 1 mpci	Yes	***
36 hpci vs 7 dpci	Yes	***
36 hpci vs 9 dpci	Yes	***
36 hpci vs 5 dpci	Yes	**
36 hpci vs 3 dpci	No	**ns**
3 dpci vs 3 mpci	Yes	***
3 dpci vs 1 mpci	Yes	***
3 dpci vs 7 dpci	Yes	***
3 dpci vs 9 dpci	Yes	***
3 dpci vs 5 dpci	Yes	**
5 dpci vs 3 mpci	Yes	***
5 dpci vs 1 mpci	Yes	*
5 dpci vs 7 dpci	No	**ns**
5 dpci vs 9 dpci	No	**ns**
9 dpci vs 3 mpci	Yes	**
9 dpci vs 1 mpci	No	**ns**
9 dpci vs 7 dpci	No	**ns**
7 dpci vs 3 mpci	Yes	*
7 dpci vs 1 mpci	No	**ns**
1 mpci vs 3 mpci	Yes	*

Table S4: Newman-Keuls Multiple Comparison Test for relative GFP^+ cell proliferation at indicated time points (Figure 1N)

Sample comparison	Significant? *P*<0.05?	Summary
24 hpci vs 3 dpci	Yes	***
24 hpci vs 5 dpci	Yes	*
24 hpci vs 36 hpci	No	ns
24 hpci vs 7 dpci	No	ns
7 dpci vs 3 dpci	Yes	***
7 dpci vs 5 dpci	Yes	*
7 dpci vs 36 hpci	No	ns
36 hpci vs 3 dpci	Yes	***
36 hpci vs 5 dpci	Yes	*
5 dpci vs 3 dpci	Yes	***

Table S5: Newman-Keuls Multiple Comparison Test for relative *serpine1*$^+$/ GFP^+ cells at indicated time points (Figure 7D)

Sample comparison	Significant? P < 0.05?	Summary
7 dpci vs 24 hpci	Yes	***
7 dpci vs 36 hpci	Yes	***
7 dpci vs 3 dpci	Yes	*
3 dpci vs 24 hpci	Yes	***
3 dpci vs 36 hpci	Yes	***
36 hpci vs 24 hpci	No	ns

Table S6: RNA-seq data of RO- *vs.* DMSO-treated wild type regenerating hearts 3 dpci (Excell file attached)

Click here to Download Table S6

Table S7: Primers used for RNA probe generation

Gene	forward	reverse
serpine1	GTT TGCTGAAGCCGTCCAGT	TCCACGCCATCCTTAGACAC
ctssb.1	GATGAAAATGCCCTCAAGCAG	AAGATAAGACGCACTTGGAT
myc-b	TTT ACC ACG GCT ACG GCA CT	CGG ATT CGC TGT CAC TAC TG
tnfrsf9a	TACGGAAAACTCAGAGTCCA	TTTGAGTATTCTCTCCCCAA
mpeg1	AACTCAGAGATCATCATGTCG	TGCCCTGATAACTACTGCTT
heg	CATTCAGGTACTGCGAACGACA	TACAACTGCGGCCATCCTC
egr1	CTTGCTGGAGATACGCTTTC	GGCTGCTGACCCGCTTGTGT
id1	CACTATCGACAACTCAACAAGCC	ACGTCACGCTTGTCATGTCCA
mylk3	GAGCCCACACATGTCCAGA	CTGTTGTTTCCATCCCCAT
tnfrsf9a	TACGGAAAACTCAGAGTCCA	TTTGAGTATTCTCTCCCCAA

Table S8: qPCR primers (*Danio rerio*)

Gene	forward	reverse
cathepsin B, a	GCACGACTGCCATACACAAG	GGCTGAGATCACACACAGGA
ctssb.1	CCAGATTCACTGGATTGGAGA	CCAACAAGAACCACAAGCAC
elf1a	CAGCTGATCGTTGGAGTCAA	TGTATGCGCTGACTTCCTTG
heg	TTGGAGGTTTCAACTGCAATAA	GCAATGACCACAATCAACAGA
her15	TCGCTCTGCTCAGAAACA	ACCACTGGCTTTCGAAT
her4.1	CAGAGAAACTCTACTGACAAACAAGC	GCTGCTGTTGATTCGCTCT
her6	GGCTTCGGAACACAGAAAGT	TGACCCAAGCTTTCGTTGA
hyal2	TTTGTCTACAGCCGCCCTAC	CAATGGTGGACACCAGATCA
klf2a	CCGTCTATTTCCACATTTTCG	TCCAGTTCATCCTTCCACCT
klf2b	CGTGGACATGGCTTTACCTT	TTGTGCTCCTCAATCTTCCA
mmp9	TGCTCTCCCAGCTGTCATC	CCACTGTAAACCCAGAACTGTCT
myc-b	TGTTTCCCTTTCCACTGAC	CTTCATCATCTTCGTCATCG
mylk3	AAGTTGAGTCGACACTGCTGAT	ACAATGCGATGGTCGAATG
rpsm	GATGGCGGACACTCAGAAC	CCAATCCAACGTTTCTGTGA
serpine1	GTCTATTCCAAGGTTCTCCAT	CTGAAAATGTCTCCAAGACC
sgpl1	CCATTATTATGAAGAATCCGAAAGA	CATCGATCGGTCAGGAATG
tcap	GGGACGATCAATGTCTCAGG	CGTCCATAAAGTCTTTGACTCATATTT
tnfrsf9a	AACTGGACTCCTTCAGGAAAAA	TCTTTTCACCAAGCGGTTTC

Table S9: qPCR primers (*Sus scrofa*)

Gene	forward	reverse
SERPINE1	TACACTGAGTTTTCCACCC	AATGAACATGCTCAGAGTG
GAPDH	ACACTCACTCTTCTACCTTTG	CAAATTCATTGTCGTACCAG

Supplementary References

Chen, J., Huang, C., Truong, L., La Du, J., Tilton, S. C., Waters, K. M., Lin, K., Tanguay, R. L. and Dong, Q. (2012). Early life stage trimethyltin exposure induces ADP-ribosylation factor expression and perturbs the vascular system in zebrafish. *Toxicology* **302**, 129-139.

Chen, J. N. and Fishman, M. C. (1996). Zebrafish tinman homolog demarcates the heart field and initiates myocardial differentiation. *Development* **122**, 3809-3816.

Gonzalez-Rosa, J. M., Martin, V., Peralta, M., Torres, M. and Mercader, N. (2011). Extensive scar formation and regression during heart regeneration after cryoinjury in zebrafish. *Development* **138**, 1663-1674.

Kanzler, B., Kuschert, S. J., Liu, Y. H. and Mallo, M. (1998). Hoxa-2 restricts the chondrogenic domain and inhibits bone formation during development of the branchial area. *Development* **125**, 2587-2597.

Kikuchi, K., Holdway, J. E., Major, R. J., Blum, N., Dahn, R. D., Begemann, G. and Poss, K. D. (2011). Retinoic acid production by endocardium and epicardium is an injury response essential for zebrafish heart regeneration. *Developmental cell* **20**, 397-404.

Larson, J. D., Wadman, S. A., Chen, E., Kerley, L., Clark, K. J., Eide, M., Lippert, S., Nasevicius, A., Ekker, S. C., Hackett, P. B. et al. (2004). Expression of VE-cadherin in zebrafish embryos: a new tool to evaluate vascular development. *Developmental dynamics : an official publication of the American Association of Anatomists* **231**, 204-213.

Lawson, N. D. and Weinstein, B. M. (2002). In vivo imaging of embryonic vascular development using transgenic zebrafish. *Developmental biology* **248**, 307-318.

Luxan, G., Casanova, J. C., Martinez-Poveda, B., Prados, B., D'Amato, G., MacGrogan, D., Gonzalez-Rajal, A., Dobarro, D., Torroja, C., Martinez, F. et al. (2013). Mutations in the NOTCH pathway regulator MIB1 cause left ventricular noncompaction cardiomyopathy. *Nature medicine* **19**, 193-201.

Munch, J., Gonzalez-Rajal, A. and de la Pompa, J. L. (2013). Notch regulates blastema proliferation and prevents differentiation during adult zebrafish fin regeneration. *Development* **140**, 1402-1411.

Poon, K. L., Liebling, M., Kondrychyn, I., Garcia-Lecea, M. and Korzh, V. (2010). Zebrafish cardiac enhancer trap lines: new tools for in vivo studies of cardiovascular development and disease. *Developmental dynamics : an official publication of the American Association of Anatomists* **239**, 914-926.

Prince, V. E., Holley, S. A., Bally-Cuif, L., Prabhakaran, B., Oates, A. C., Ho, R. K. and Vogt, T. F. (2001). Zebrafish lunatic fringe demarcates segmental boundaries. *Mechanisms of development* **105**, 175-180.

Rohr, S., Otten, C. and Abdelilah-Seyfried, S. (2008). Asymmetric involution of the myocardial field drives heart tube formation in zebrafish. *Circulation research* **102**, e12-19.

Scheer, N., Groth, A., Hans, S. and Campos-Ortega, J. A. (2001). An instructive function for Notch in promoting gliogenesis in the zebrafish retina. *Development* **128**, 1099-1107.

Susaki, E. A., Tainaka, K., Perrin, D., Kishino, F., Tawara, T., Watanabe, T. M., Yokoyama, C., Onoe, H., Eguchi, M., Yamaguchi, S. et al. (2014). Whole-brain imaging with single-cell resolution using chemical cocktails and computational analysis. *Cell* **157**, 726-739.

Vermot, J., Forouhar, A. S., Liebling, M., Wu, D., Plummer, D., Gharib, M. and Fraser, S. E. (2009). Reversing blood flows act through klf2a to ensure normal valvulogenesis in the developing heart. *PLoS biology* **7**, e1000246.

Westin, J. and Lardelli, M. (1997). Three novel Notch genes in zebrafish: implications for vertebrate Notch gene evolution and function. *Development genes and evolution* **207**, 51-63.

Wong, K. S., Rehn, K., Palencia-Desai, S., Kohli, V., Hunter, W., Uhl, J. D., Rost, M. S. and Sumanas, S. (2012). Hedgehog signaling is required for differentiation of endocardial progenitors in zebrafish. *Developmental biology* **361**, 377-391.

Yelon, D., Ticho, B., Halpern, M. E., Ruvinsky, I., Ho, R. K., Silver, L. M. and Stainier, D. Y. (2000). The bHLH transcription factor hand2 plays parallel roles in zebrafish heart and pectoral fin development. *Development* **127**, 2573-2582.

Yoshinari, N., Ishida, T., Kudo, A. and Kawakami, A. (2009). Gene expression and functional analysis of zebrafish larval fin fold regeneration. *Developmental biology* **325**, 71-81.

Zhang, R., Han, P., Yang, H., Ouyang, K., Lee, D., Lin, Y. F., Ocorr, K., Kang, G., Chen, J., Stainier, D. Y. et al. (2013). In vivo cardiac reprogramming contributes to zebrafish heart regeneration. *Nature* **498**, 497-501.

Supplementary Movies

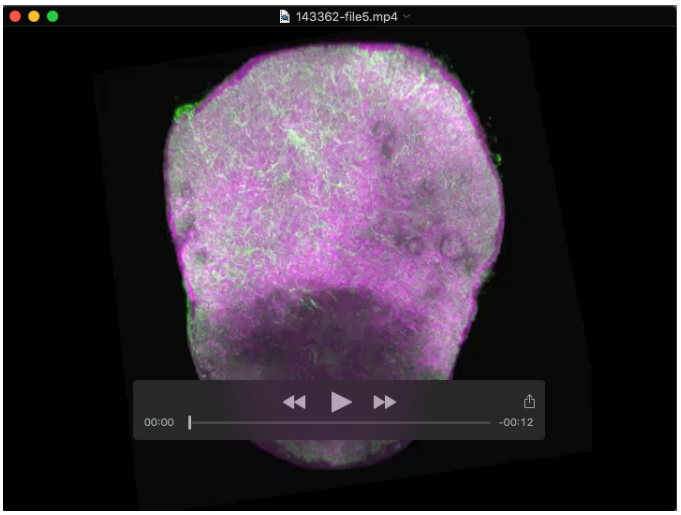

Movie 1: IMARIS volume rendering of a whole mount *ET33-mi60a* (green); *myl7:mRFP*(magenta) cryoinjured transgenic heart at 24 hpci.

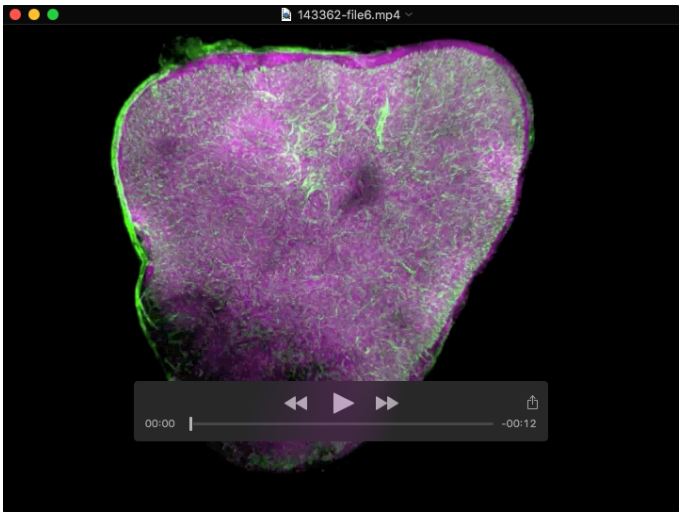

Movie 2: IMARIS volume rendering of a whole mount *ET33-mi60a* (green); *myl7:mRFP*(magenta) cryoinjured transgenic heart at 36 hpci.

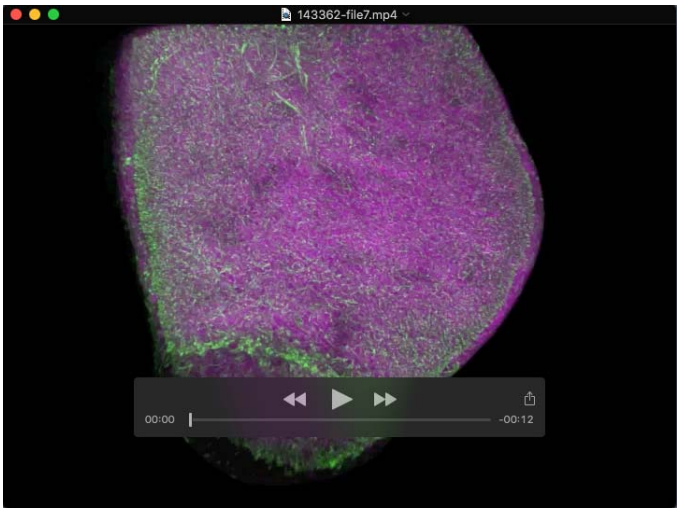

Movie 3: IMARIS volume rendering of a whole mount *ET33-mi60a* (green); *myl7:mRFP*(magenta) cryoinjured transgenic heart at 3 dpci.

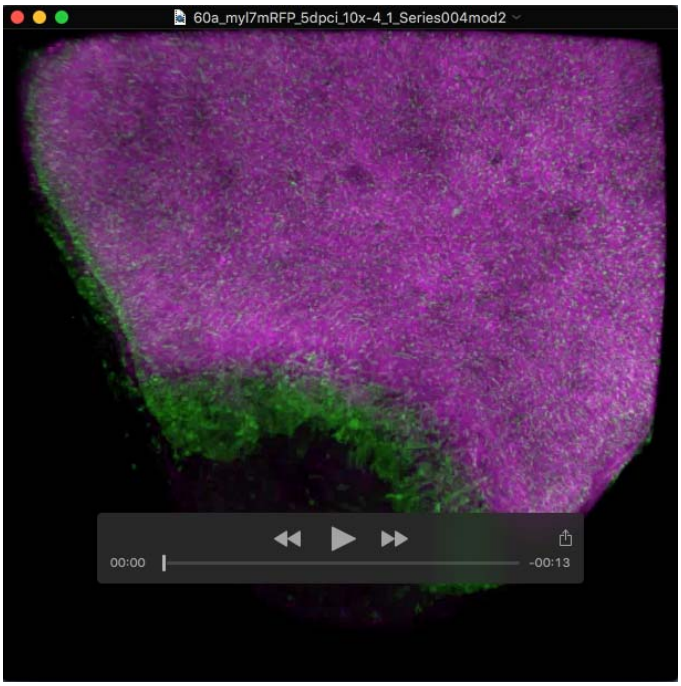

Movie 4: IMARIS volume rendering of a whole mount *ET33-mi60a* (green); *myl7:mRFP*(magenta) cryoinjured transgenic heart at 5 dpci.

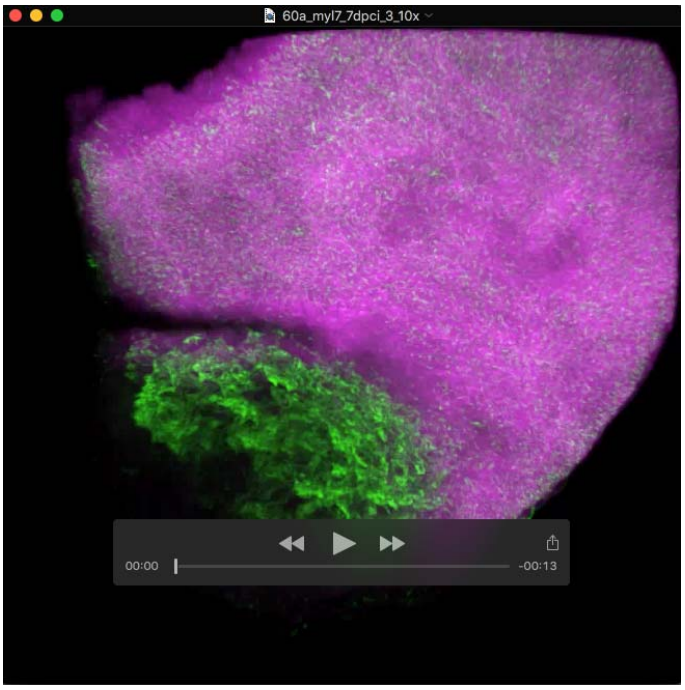

Movie 5: IMARIS volume rendering of a whole mount *ET33-mi60a* (green); *myl7:mRFP*(magenta) cryoinjured transgenic heart at 7 dpci.

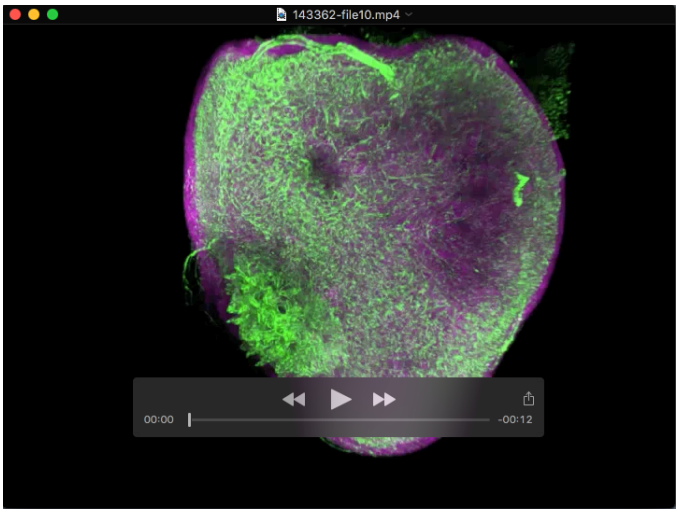

Movie 6: IMARIS volume rendering of a whole mount *ET33-mi60a* (green); *myl7:mRFP*(magenta) cryoinjured transgenic heart at 9 dpci.

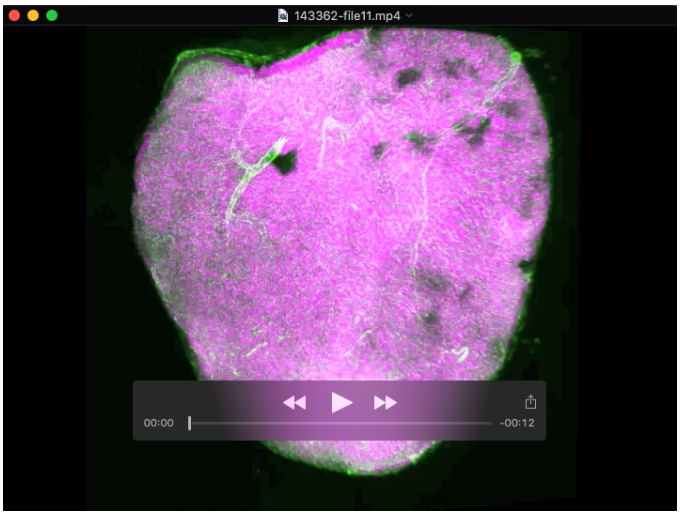

Movie 7: IMARIS volume rendering of a whole mount *ET33-mi60a* (green); *myl7:mRFP*(magenta) cryoinjured transgenic heart at 1 mpci.

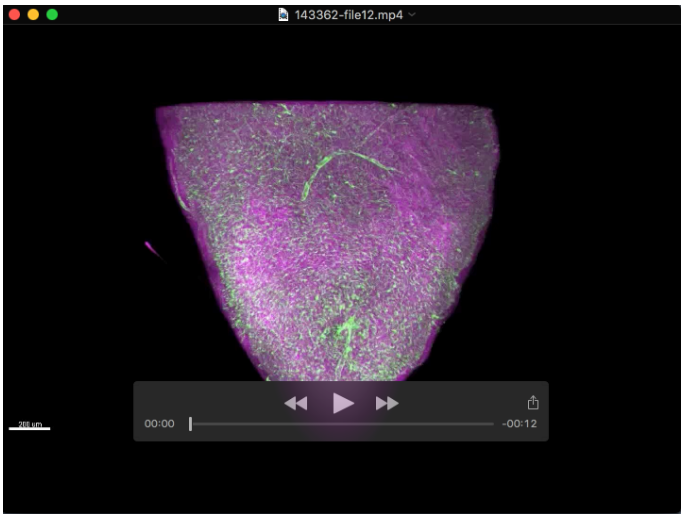

Movie 8: IMARIS volume rendering of a whole mount *ET33-mi60a* (green); *myl7:mRFP*(magenta) cryoinjured transgenic heart at 3 mpci.

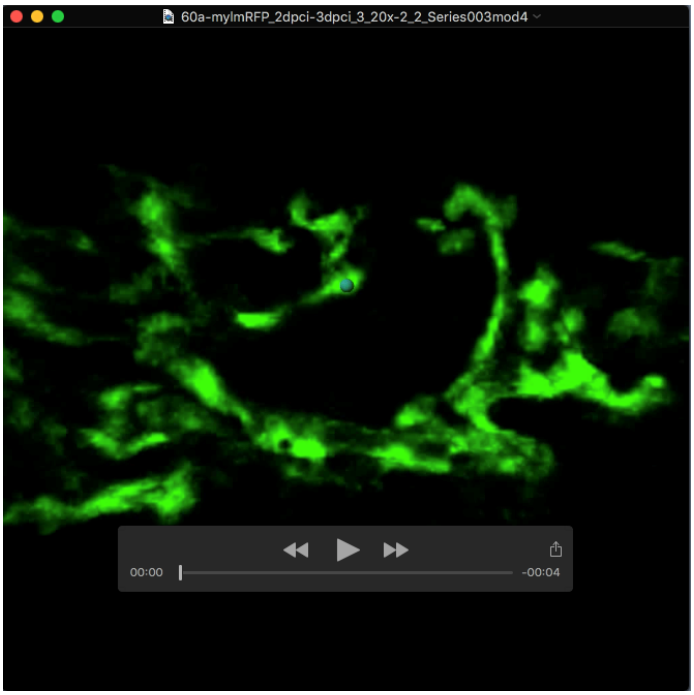

Movie 9: Confocal 3D time-lapse movie of endocardial cells of a selected area within the injury site in *ET33-mi60a* (green); *myl7:mRFP* (magenta) cryoinjured transgenic heart at around 56 hpci. Individual cells migrate and change their collocation. Still images can be found in Figures 2H.

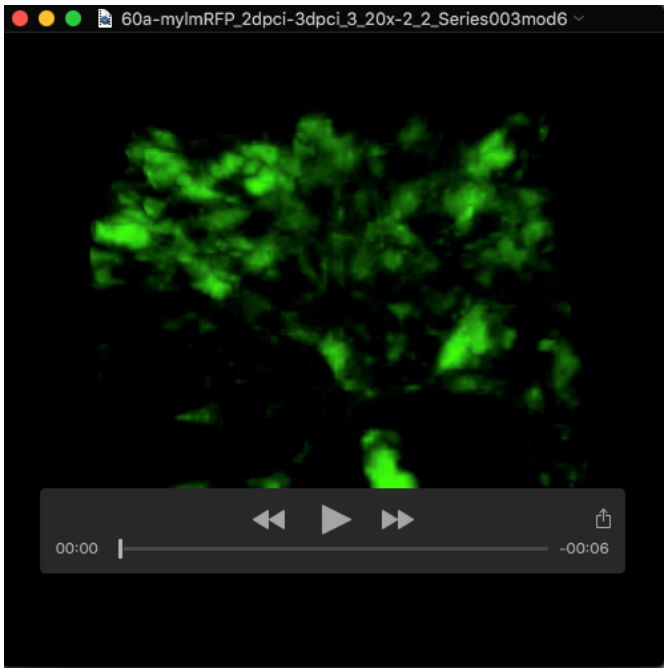

Movie 10: Confocal 3D time-lapse movie of endocardial cells of a selected area within the injury site in *ET33-mi60a* (green); *myl7:mRFP* (not shown) cryoinjured transgenic heart at around 56 hpci. Individual cells migrate and send out filopodia-like protrusions. Still images can be found in Figures 2I.